

Tectonics

RESEARCH ARTICLE

10.1029/2019TC005924

Key Points:

- Regionally extensive subsurface data are used to quantify basin-wide strain behavior during early stages of continental rifting
- Variable magnitude and rate of extension-related strain affect the structural development of upper crustal fault systems and host array
- Three-dimensional strain behavior during initial continental rift phases might be more complex than previously assumed

Supporting Information:

- Supporting Information S1

Correspondence to:

J. S. Claringbould,
jsclaring@eri.u-tokyo.ac.jp

Citation:

Claringbould, J. S., Bell, R. E., Jackson, C. A.-L., Gawthorpe, R. L., & Odinsen, T. (2020). Pre-breakup extension in the northern North Sea defined by complex strain partitioning and heterogeneous extension rates. *Tectonics*, 39, e2019TC005924. <https://doi.org/10.1029/2019TC005924>

Received 21 OCT 2019

Accepted 15 JUN 2020

Accepted article online 22 JUN 2020

©2020. The Authors.

This is an open access article under the terms of the Creative Commons Attribution License, which permits use, distribution and reproduction in any medium, provided the original work is properly cited.

Pre-breakup Extension in the Northern North Sea Defined by Complex Strain Partitioning and Heterogeneous Extension Rates

Johan S. Claringbould^{1,2} , Rebecca E. Bell¹ , Christopher A.-L. Jackson¹ , Robert L. Gawthorpe³ , and Tore Odinsen⁴

¹Basins Research Group (BRG), Department of Earth Science and Engineering, Imperial College London, London, UK, ²Now at Earthquake Research Institute, The University of Tokyo, Tokyo, Japan, ³Department of Earth Science, University of Bergen, Bergen, Norway, ⁴Equinor ASA, Bergen, Norway

Abstract The early stages of continental rifting are accommodated by the growth of upper crustal normal fault systems that are distributed relatively evenly across the rift width. Numerous fault systems define fault arrays, the kinematics of which are poorly understood due to a lack of regional studies drawing on high-quality subsurface data. Here we investigate the long-term (~150 Myr) growth of a rift-related fault array in the East Shetland Basin, northern North Sea, using a regionally extensive subsurface data set comprising 2-D and 3-D seismic reflection surveys and 107 boreholes. We show that rift-related strain during the pre-Triassic to Middle Triassic was originally distributed across several subbasins. The Middle to Late Triassic saw a decrease in extension rate (~14 m/Myr) as strain localized in the western part of the basin. Early Jurassic strain initially migrated eastward, before becoming more diffuse during the main, Middle-to-Late Jurassic rift phase. The highest extension rates (~89 m/Myr) corresponded with the main rift event in the East Shetland Basin, before focusing of strain within the rift axis and ultimate abandonment of the East Shetland Basin in the Early Cretaceous. We also demonstrate marked spatial variations in timing and magnitude of slip along strike of major fault systems during this protracted rift event. Our results imply that strain migration patterns and extension rates during the initial, prebreakup phase of continental rifting may be more complex than previously thought; this reflects temporal and spatial changes in both thermal and mechanical properties of the lithosphere, in addition to varying extension rates.

1. Introduction

Continental rifting is accommodated by the growth of upper crustal (i.e., top 5–10 km of the crustal structure) normal faults. Resolving the dynamics of continental rifting is important because normal faults control rift geomorphology and landscape development in time and space, and the erosion, transport, and storage of sediment (Gawthorpe & Leeder, 2000). Our current understanding of continental rift dynamics is largely based on studies focused on examples that have proceeded to full plate rupture and continental breakup (e.g., Brun, 1999; Gibbs, 1984; Huismans & Beaumont, 2007; Nagel & Buck, 2007; Péron-Pinvidic et al., 2013; Ziegler & Cloetingh, 2004), supplemented by those concentrating on failed rifts. The latter tend to focus on specific aspects or time periods of the rifting process, such as local and regional migration of extension-related strain (e.g., Behn et al., 2002; Bell et al., 2014; Corti et al., 2013; Cowie et al., 2005; Naliboff & Buitert, 2015), the influence of crustal composition and (preexisting) structures on fault and rift geometry (e.g., Duffy et al., 2015; Henstra et al., 2019; Paton, 2006; Phillips et al., 2016; Whipp et al., 2014), and/or the effect of the initial lithospheric conditions (e.g., crustal thickness and thermal state) on rift development (e.g., Buck, 1991, 2006; Corti et al., 2003; Odinsen et al., 2000).

The way in which strain is accumulated during lithospheric stretching (e.g., varying magnitude and rates), and how this relates to the overall geometry of the resultant rift, has also been extensively studied (e.g., Bassi, 1995; Behn et al., 2002; England, 1983; Kusznir & Park, 1987; Naliboff et al., 2017; Van Wijk & Cloetingh, 2002). Numerical and physical models of rift development, which simulate the formation of upper crustal deformation, do not, however, commonly consider how strain behaves in three dimensions. This often reflects the limited spatial and temporal resolution of such models, which allows them to only predict the patterns of strain migration in two dimensions (e.g., toward or away from the rift axis) (e.g., Behn

et al., 2002; Cowie et al., 2000; Huismans et al., 2001; McClay, 1990; Nagel & Buck, 2007; Naliboff et al., 2017; Ziegler & Cloetingh, 2004). However, observations from individual faults or *fault systems* (i.e., a kinematically linked group of fault segments that are several km to tens of kilometers long) suggest that the overall accumulation of rift-related strain can be rather complex in three dimensions due to, for example, fault segment interaction and/or the composition and structure of the upper crust (e.g., Cowie et al., 2000; Duffy et al., 2015; Jackson et al., 2017; Nixon et al., 2014; Putz-Perrier & Sanderson, 2008; Soliva et al., 2006; Walsh et al., 2003; Whipp et al., 2014). Recent studies of relatively young (<5 Myr old), still-active rifts (e.g., Gulf of Corinth Rift, Bell et al., 2009; Ford et al., 2013; Nixon et al., 2016) and inactive rifts (e.g., southern South African extensional system, Paton, 2006; northern North Sea, Claringbould et al., 2017) suggest that the initial phase of upper crustal stretching is distributed across a wide zone. During this early phase of continental rifting, diffuse extension is associated with the diachronous growth of individual fault systems that make up the larger, rift-related *fault array* (i.e., a kinematically linked group of fault systems that are tens to hundred kilometers of length and typically cover one margin of a rift). Péron-Pinvidic et al. (2013) argue that rift-related strain migrates during the transition from diffuse stretching and thinning of the upper crust, to hyperextension and mantle exhumation, a progression that may also be linked to an increase in extension rate (e.g., Brune et al., 2016; Naliboff et al., 2017).

The way in which strain rate controls rift geometry is closely related to the way in which heat is generated and transferred during extension. England (1983) shows that during extension, the lithosphere increases in strength because rift-related continental thinning will result in the lithosphere cooling as it is brought closer to the surface. If the extension rate is relatively slow, this so-called synrift cooling will prevent further extension, causing the locus of maximum strain to shift laterally, allowing the rift to widen (Bassi, 1995). However, when the extension rate is relatively fast, synrift cooling will not occur, and necking and rift narrowing will instead take place (Kuszniir & Park, 1987). This proposed relationship between extension rate and the resulting rift pattern has since been observed in numerous 2-D, lithospheric-scale models (e.g., Brune et al., 2016; Naliboff et al., 2017; Tetreault & Buitier, 2018; Van Wijk & Cloetingh, 2002). However, we have yet to use observations from natural rifts to document how and the timescale over which early rift-related strain is recorded by the growth of upper crustal fault arrays nor have we determined how changes in bulk extension magnitude and rate affect the temporal evolution of rift-wide strain. The increased complexity and inferred realism of relatively recent numerical models has essentially not been matched by an increased level of observational details to test their predictions.

Determining the geometry and growth of crustal-scale ($\sim 10,000 \text{ km}^2$) normal fault arrays, as opposed to individual fault systems, requires extensive, high-quality, subsurface data. To this end, we focus on the East Shetland Basin, northern North Sea (Figure 1). The northern North Sea represents a failed rift basin that developed in response to protracted extension spanning $\sim 150 \text{ Myr}$ (Færseth, 1996). The East Shetland Basin, located on the western margin of the North Viking Graben, contains a large fault array that is part of the wider northern North Sea rift system (Figure 1). We use a large subsurface data set comprising long ($\sim 75 \text{ km}$), deep-imaging ($\sim 8\text{-s}$ two-way time, TWT) regional 2-D seismic reflection profiles, multiple, merged 3-D seismic surveys (covering $\sim 10,000 \text{ km}^2$) that image to moderate depths (4.5–6.5-s TWT), and 107 hydrocarbon exploration and production boreholes. Our data set allows a relatively high resolution (i.e., as little as $\sim 10\text{-Myr}$ temporal scale and a few hundred-of-meters spatial scale) examination of (i) the long-term ($\sim 150 \text{ Myr}$) migration of rift-related strain across a large fault array ($\sim 10,000 \text{ km}^2$) and (ii) temporal changes in the magnitude and rate of extension at the subbasin scale, which we can then compare to rift-scale variations in these parameters. Our analysis provides an improved understanding of how rift-related strain accumulates during the initial, prebreakup phase of continental rifting, and the effect that heterogeneous extension magnitudes and rates have on the resulting rift geometry. We also use our results to infer how the thermal and mechanical properties of the lithosphere varied through time during protracted extension. Finally, our study of a natural rift allows us to critically test the predictions of physical and numerical models of continental extension.

2. Geological Setting

The East Shetland Basin is located in the northern North Sea, offshore western Norway, on the western margin of the North Viking Graben (Figure 1). The present geometry of the basin is characterized by large ($>25\text{-}$

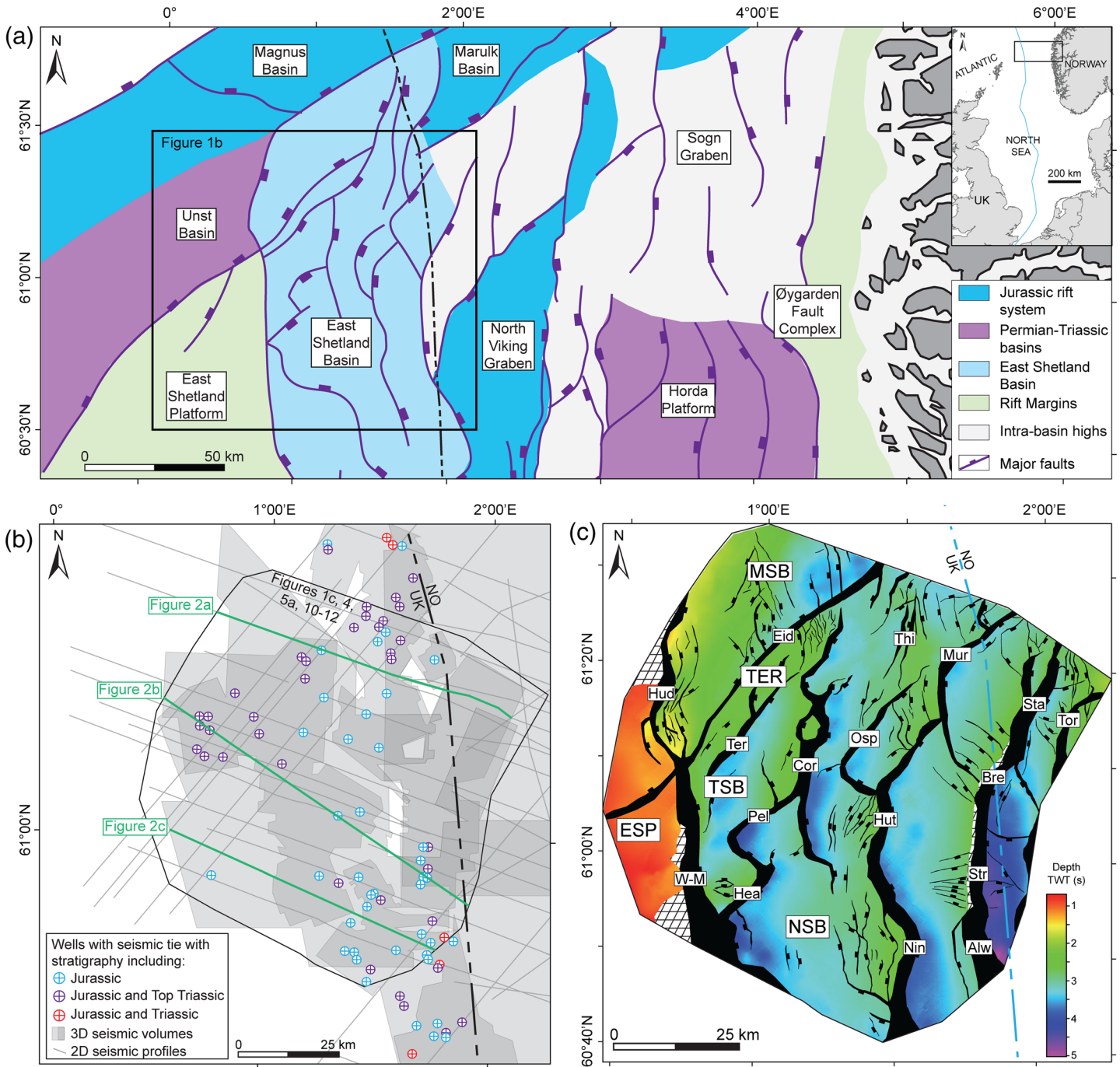


Figure 1. (a) Major tectonic elements of the northern North Sea (after Bell et al., 2014; Færseth, 1996). (b) Outlines of data set used for this study. All wells are tied to the seismic data and contain stratigraphic data for the Jurassic (blue), Jurassic and Top Triassic (purple), and Jurassic and Triassic (red). (c) Time structure map of the Top Lunde Formation with major structural elements and faults systems: Alw = Alwyn Fault System, Bre = Brent Fault System, Cor = Cormorant Fault System, Eid = Eider Fault System, ESP = East Shetland Platform, Hea = Heather Fault System, Hud = Hudson Fault System, Hut = Hutton Fault System, MSB = Magnus Subbasin, Mur = Murchison Fault System, Nin = Ninian Fault System, NSB = Ninian Subbasin, Osp = Osprey Fault System, Pel = Pelican Fault System, Sta = Statfjord Fault System, Str = Strathspey Fault System, TER = Tern-Eider Ridge, Ter = Tern Fault System, TSB = Tern Subbasin, Thi = Thistle Fault System, Tor = Tordis Fault System, W-M = West Margin Fault System. The faults systems and structural features are named after the adjacent hydrocarbon bearing fields. Modified after Claringbould et al. (2017).

km length), N-S to NE-SW striking, east dipping normal fault systems that bound 15- to 25-km-wide half-grabens (Figures 1c and 2) that developed during protracted, pre-Triassic-to-Late Jurassic rifting (~150 Myr) (e.g., Claringbould et al., 2017; Ravnås et al., 2000). Based on the interpretation of regional 2-D seismic reflection lines, flexural backstripping, and tectonostratigraphic forward modeling, two main rift phases were classically identified: Permian-Triassic and Late Jurassic (e.g., Badley et al., 1988; Færseth, 1996; Lee & Hwang, 1993; Thomas & Coward, 1995), with the magnitude of extension varying between them (e.g., Odinsen et al., 2000; Roberts et al., 1993, 1995). However, seismic-stratigraphic analysis of borehole-constrained 3-D seismic reflection data sets indicates that extension and active faulting actually continued into the Early Cretaceous (140–145 Ma; Valanginian-Berriasian), with strain eventually focusing on fault systems bounding the eastern margin of the East Shetland Basin (Bellingham & White, 2000; see also Cowie et al., 2005; Færseth et al., 1995; and McLeod et al., 2002). Strain localization on these structures was associated with overall rift narrowing and ultimately abandonment of the East Shetland Basin (Cowie et al., 2005; Phillips et al., 2019).

The increasing availability of high-quality 3-D seismic reflection data has permitted a more detailed analysis of the geometry and growth of the individual fault systems in the East Shetland Basin. Even then, most studies consider time interval that are relatively short (e.g., Late Jurassic; ~18 Myr) given that, together, the various Permian-to-Early Cretaceous rift phases or pulses spanned ~150 Myr (e.g., Strathspey-Brent-Statfjord half graben, Cowie et al., 2005; Murchison-Statfjord North Fault, McLeod et al., 2000, 2002; eastern East Shetland Basin, Tomasso et al., 2008; Triassic Ninian and Alwyn North fields, Young et al., 2001). Because they focus on relatively small areas and/or for only a relatively short part of the much longer rift episode, these studies can also only show how strain accumulates during the development of individual fault systems; the longer-term (~150 Myr) dynamics of the larger host fault array remains unknown.

In this study we develop the ideas of Claringbould et al. (2017) and Ravnås et al. (2000), who show that rifting in the northern North Sea was protracted not punctuated. Ravnås et al. (2000) propose that the northern North Sea experienced Permian-to-Early Triassic and Middle-to-Late Jurassic rift episodes that were separated by an intervening, Middle Triassic-to-Middle Jurassic *interrift* period characterized by more diffuse extension. Claringbould et al. (2017) qualitatively describe the entire pre-Triassic-to-Late Jurassic evolution of the fault array in the East Shetland Basin. They argue that although preexisting upper crustal structures may have locally influenced the geometry and growth subsequent rift-related structures, the more extensive, lithosphere-scale, thermal, and rheologic heterogeneities served to somewhat dilute their control on the overall rift geometry. This study builds on Claringbould et al. (2017) by quantifying the ~150-Myr evolution of the East Shetland Basin fault array during eight time intervals that individually span ~6–45 Myr. Because our seismic reflection data set does not image structures associated with the very latest stage of extension (i.e., Early Cretaceous; post-145 Ma), we do not explicitly consider the detailed growth of fault systems most active at this time. We do, however, place our study within the more regional, late synrift-to-early postrift tectonostratigraphic framework erected by other authors (Bellingham & White, 2000; Cowie et al., 2005; McLeod et al., 2000; Phillips et al., 2019).

3. Data and Methods

3.1. Seismic Reflection and Well Data

We use an extensive data set comprising 2-D and 3-D time-migrated seismic reflection surveys that were collected between 2006 and 2012 (Figure 1b). More specifically, we use four, partly overlapping, 3-D seismic “merged-surveys,” which cover almost the whole East Shetland Basin (~10,000 km²). These data image to depths of 4.5- to 6.5-s TWT (6–8 km) and have a 12.5 × 12.5 m or 25 × 25 m inline and crossline spacing. We also use long (~75-km length), 2-D seismic profiles that trend either NNE or WNW, image to depths of ~8-s TWT (~10 km) and have a line spacing of ~5 km (Figure 1b). Seismic data quality ranges from excellent for some of the 3-D surveys to moderate for some of the 2-D profiles. In addition to the seismic reflection data, we use 107 hydrocarbon exploration wells to determine the age of the basin fill, of which 82 are tied to the seismic data through the construction of synthetic seismograms (Figure 3).

3.2. Seismic Interpretation and Fault System Analysis

We interpret nine key seismic horizons across an area of ~6,800 km² (pre-Triassic to the Base Cretaceous Unconformity; Figures 2 and 3). Our primary interpretation is based on the 3-D surveys given they allow

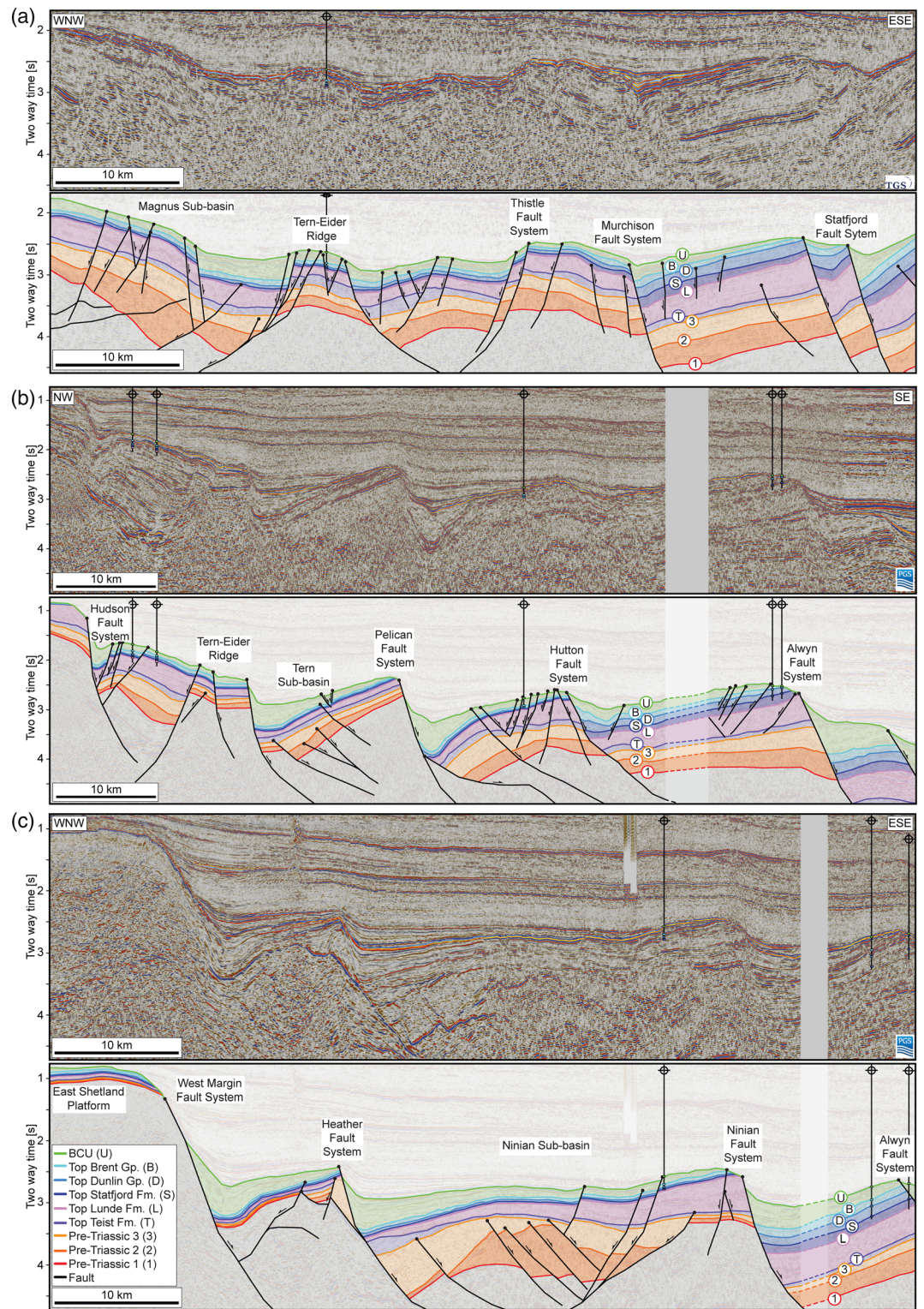


Figure 2. Uninterpreted and interpreted time-migrated seismic reflection profiles crossing the study area in the (a) north, (b) center, and (c) south. The seismic profiles including well penetrations and major faults and structural features. See Figure 1b for locations. Modified after Claringbould et al. (2017).

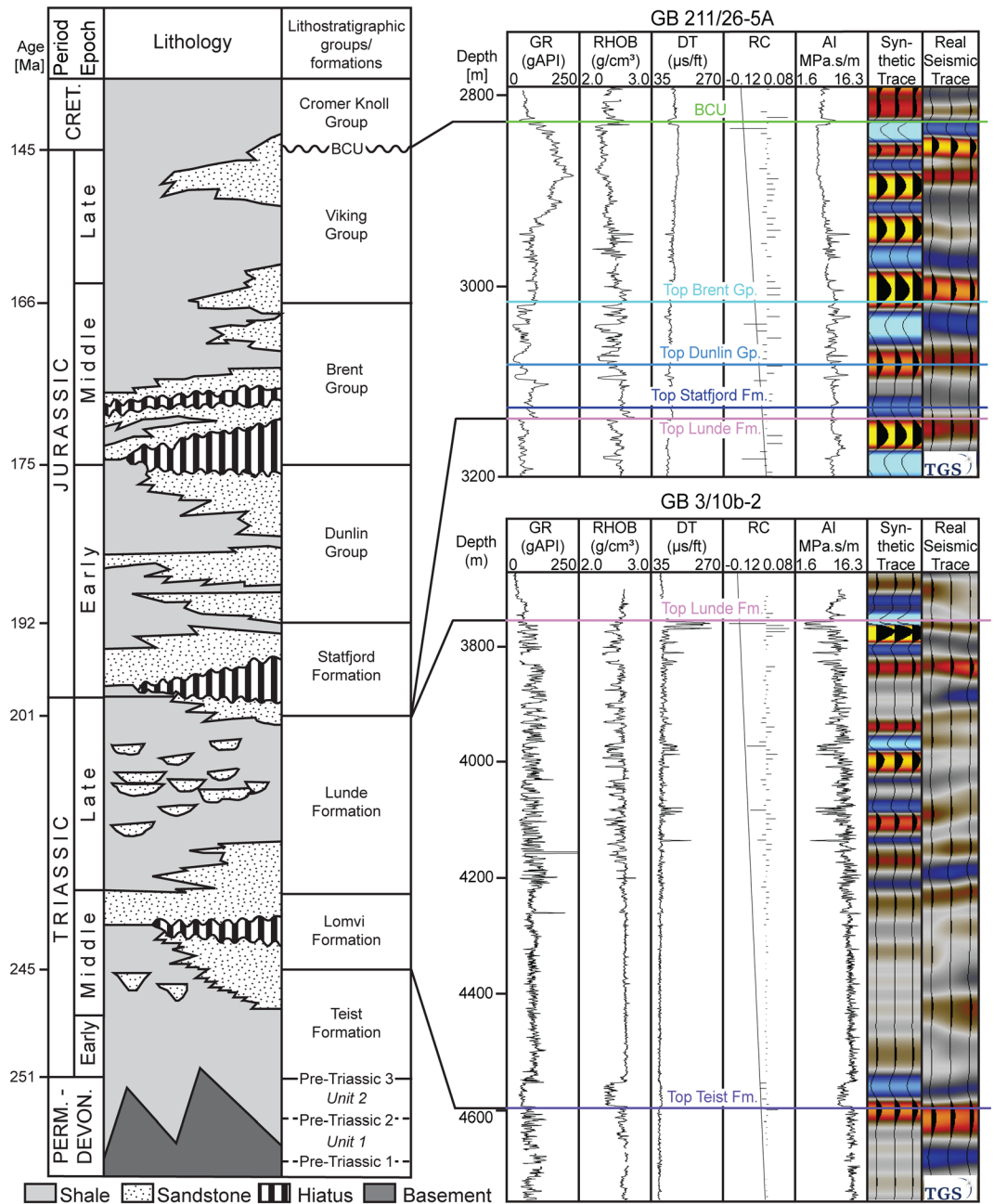


Figure 3. Stratigraphic column of the pre-Triassic to Cretaceous in the East Shetland Basin showing lithology (after Færseth, 1996), lithostratigraphic groups/formations and ages, and the interpreted horizons and synthetic well ties (modified after Claringbould et al., 2017). Depth = TVD, GR = gamma ray, RHOB = density, DT = sonic, RC = reflection coefficient, AI = acoustic impedance.

us to (i) construct a detailed 3-D view of the present basin structure, (ii) compile time thickness maps that reveal fault-driven variations in subsidence and uplift, and (iii) extract throw and stratigraphic thickness measurements at any position along the fault systems forming part of the larger, rift-related fault array. We also use 2-D seismic profiles to correlate key seismic horizons between the 3-D surveys. With the exception of the pre-Triassic horizons, all of these horizons are tied to the wells (Figures 1b, 2, and 3). The three pre-Triassic horizons are picked based on their continuous, high-amplitude seismic character. Patruno and Reid (2017) use well data to identify Permian-Triassic to Devonian rift basins on the East Shetland Platform, which is located a few tens of kilometers SW of our study area (Figure 1a); however,

we cannot directly constrain the ages of the pre-Triassic reflections in the East Shetland Basin; thus, we name them Pre-Triassic 1, 2, and 3 (see Claringbould et al., 2017, for a full description of how these horizons were interpreted).

Our seismic mapping allows us to constrain the growth of major fault systems; these are defined as those that are >3 km long, offset at least pre-Triassic deposits, and have >200 m (>120 ms) of throw (Figure 1c). Such fault systems accommodate the majority of the rift-related strain (e.g., Fossen, 2010). Throw data are based on horizon cutoff information collected on fault normal seismic profiles that are spaced every ~625 m; this amounted to >14,000 values along 34 fault systems, which have a combined length of 535 km (Figure 4). This spatial resolution of analysis is considered sufficient to analyze strain accumulation across the entire fault array during eight time periods that span 6–45 Myr over an ~150-Myr time period (Figure 3). The horizon cutoff information is depth converted using the average time-depth relationship derived from 79 of our 107 wells.

3.3. Fault Array Analysis

Expansion indices (EIs) are used to constrain temporal variations in fault system activity and basin-wide extension magnitude (e.g., Bouroullec et al., 2004; Cartwright et al., 1998; Jackson et al., 2017; Jackson & Rotevatn, 2013; Lewis et al., 2013; Reeve et al., 2015; Thorsen, 1963) (Figure 4). EI represents the ratio between the vertical (i.e., stratigraphic) thickness of time-equivalent hanging wall and footwall strata (see supporting information). We also use throw backstripping to determine how strain accumulates along strike of individual fault systems and across the fault array (e.g., Jackson et al., 2017) (see supporting information). With the exception of the pre-Triassic units, we also calculate slip rates along the individual fault systems; this allows us to link temporal variations in local slip rate to more regional variations in strain accumulation accommodated by the larger fault array (see supporting information). The fault slip rate represents the backstripped displacement over time and is quoted in m/Myr. Because lithostratigraphic horizons do not necessarily represent chronostratigraphic surfaces (i.e., absolute timelines), we use the average absolute ages of the lithostratigraphic boundaries from the wells across the East Shetland Basin to estimate horizon ages and thus fault slip rates (Figure 3) (see supporting information).

In addition to analyzing 34 major fault systems, we sum strain along three transect lines to investigate basin-scale strain trends as rifting progressed (Figure 5). We did this on three approximately NW trending transects drawn approximately orthogonal to the analyzed fault systems; these transects covered the north, center, and south of the basin (Figure 5a). Where a transect line crosses one of the analyzed fault systems, we calculate the horizontal extension for each time period (see supporting information). These values are then summed per time period along each transect (north, center, or south) and, additionally, by region (western, central, or eastern), to show how strain accumulated in time and space (Figure 5b) (see supporting information). Furthermore, we calculate the magnitude of extension (i.e., extension factor or β factor) along the three transect lines for each time period. With the exception of the age-unconstrained pre-Triassic units, we calculated extension rates along the three transects to again analyze how strain accumulated in time and space (see supporting information) (Figures 5c and 5d). Similar to the approach used to constrain fault slip rates, we used the average absolute ages of the lithostratigraphic boundaries from the wells across the basin to estimate the extension rates (see supporting information) (Figure 5d).

Figures 6–9 show how EI and backstripped throw vary along strike of four of the largest, longest-lived fault systems that accommodated most rift-related strain (Eider, Ninian-Hutton, Cormorant, and Osprey Fault Systems; Figure 10); these data illustrate how the growth of these systems relate to the overall, basin-scale pattern of strain accumulation across the entire fault array (Figures 4 and 5). We also undertake throw-depth (T-z) analyses at specific points along these fault systems to assess how strain accumulated along their lengths (Figure 10) (e.g., Jackson et al., 2017).

Our fault analysis methods are based on several assumptions and are associated with some uncertainties. First, we note that sediment compaction may cause our measurements of fault throw to be 5–15% less than their true, near-surface, preburial values (Giba et al., 2012; Taylor et al., 2008). However, when considering our study area, we note that the thickness of sediment overburden above the analyzed fault systems is fairly constant; we therefore believe that the overall *patterns* of present-day throw will be represented of their near-surface, preburial values (cf. Reeve et al., 2015; Whipp et al., 2014). Second, our use of time thickness maps

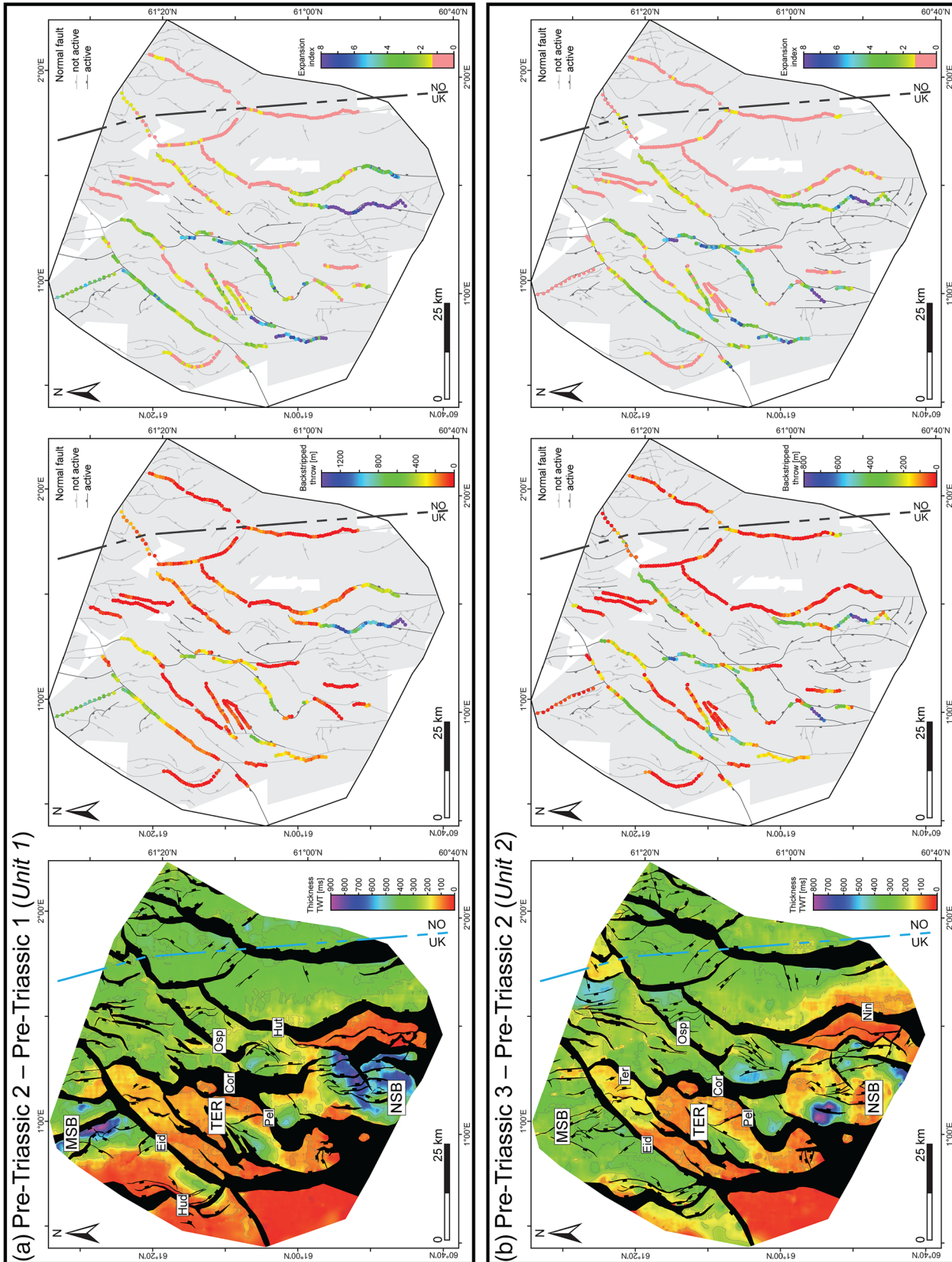


Figure 4. Isochrons overlain by fault polygons that offset the top surface (left) with line drawing of faults over outline of 3-D seismic data coverage (gray polygons) overlain by the calculated backstripped throw (middle), and expansion index (right) during the deposition of (a) Unit 1, (b) Unit 2, (c) Teist Formation, (d) Lomvi and Lunde formations, (e) Stafford Formation, (f) Dunlin Group, (g) Brent Group, and (h) Viking Group. Isochron colors are based on the maximum and minimum thickness value in ms TWT per isochron. Contour interval on all the isochrons is 100-ms TWT. Hatched areas show locations where the upper horizon is eroded. See caption of Figure 1 for abbreviated fault systems and structural features. See Figure 1c for location.

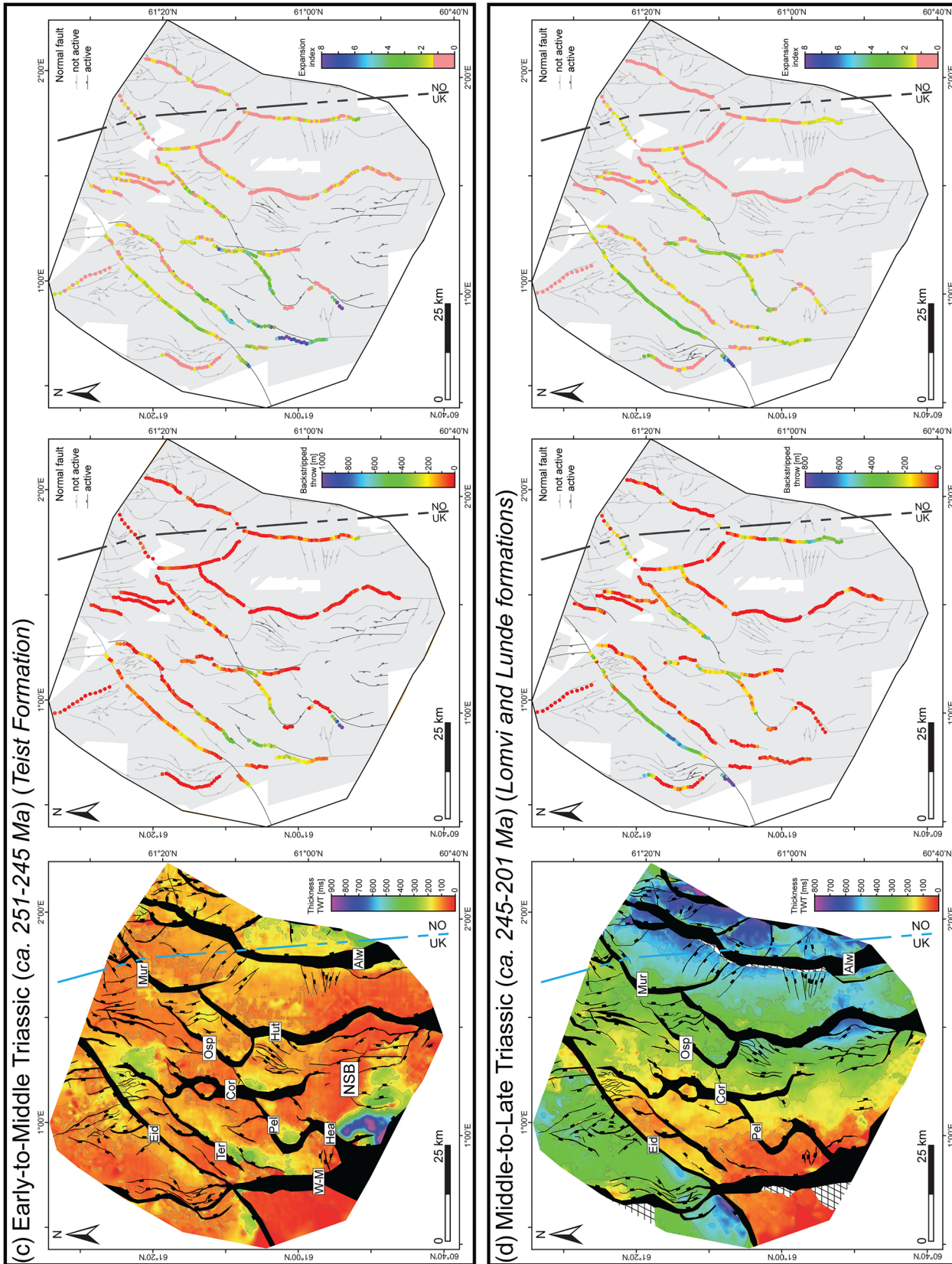


Figure 4. (Continued)

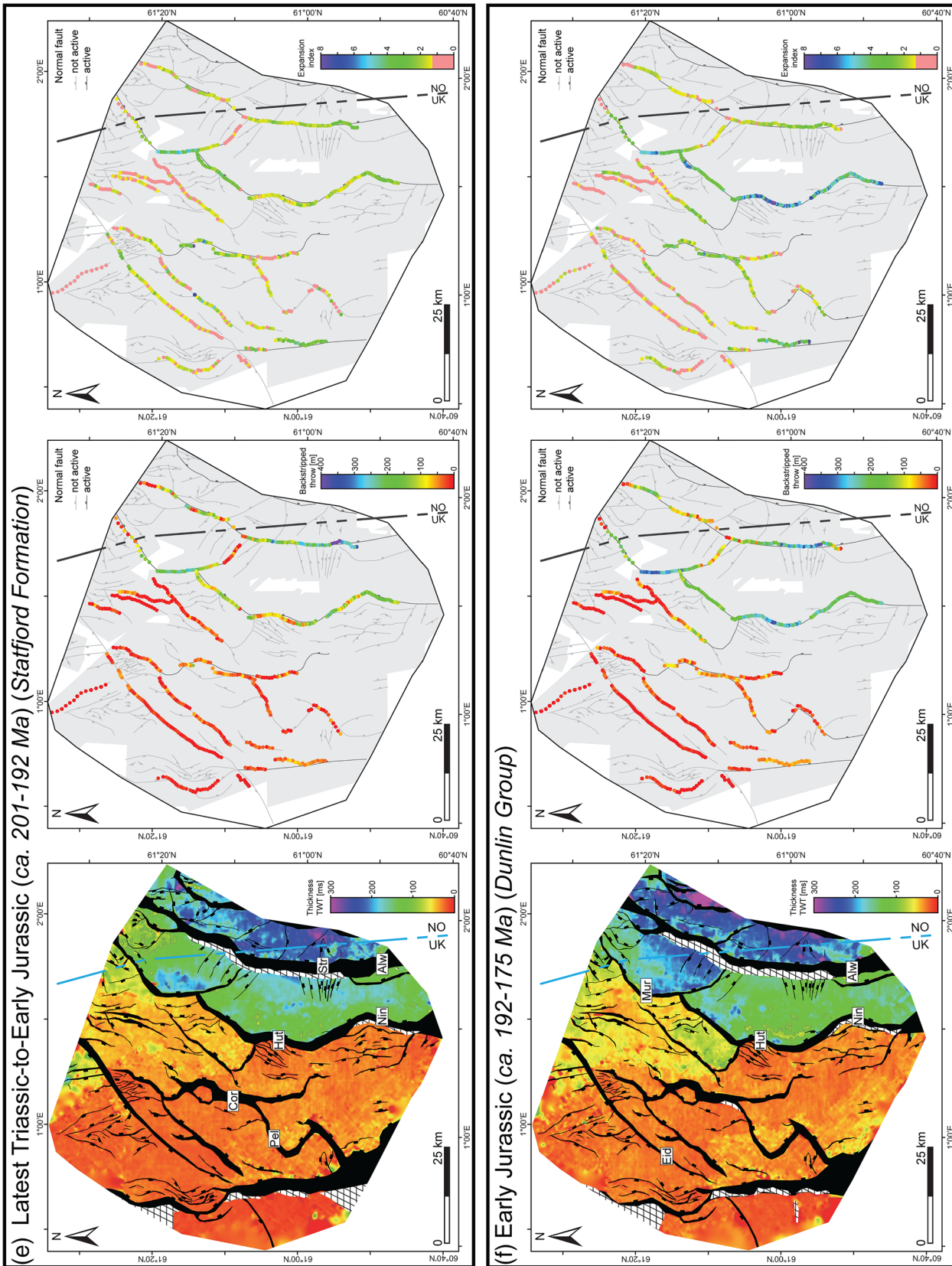


Figure 4. (Continued)

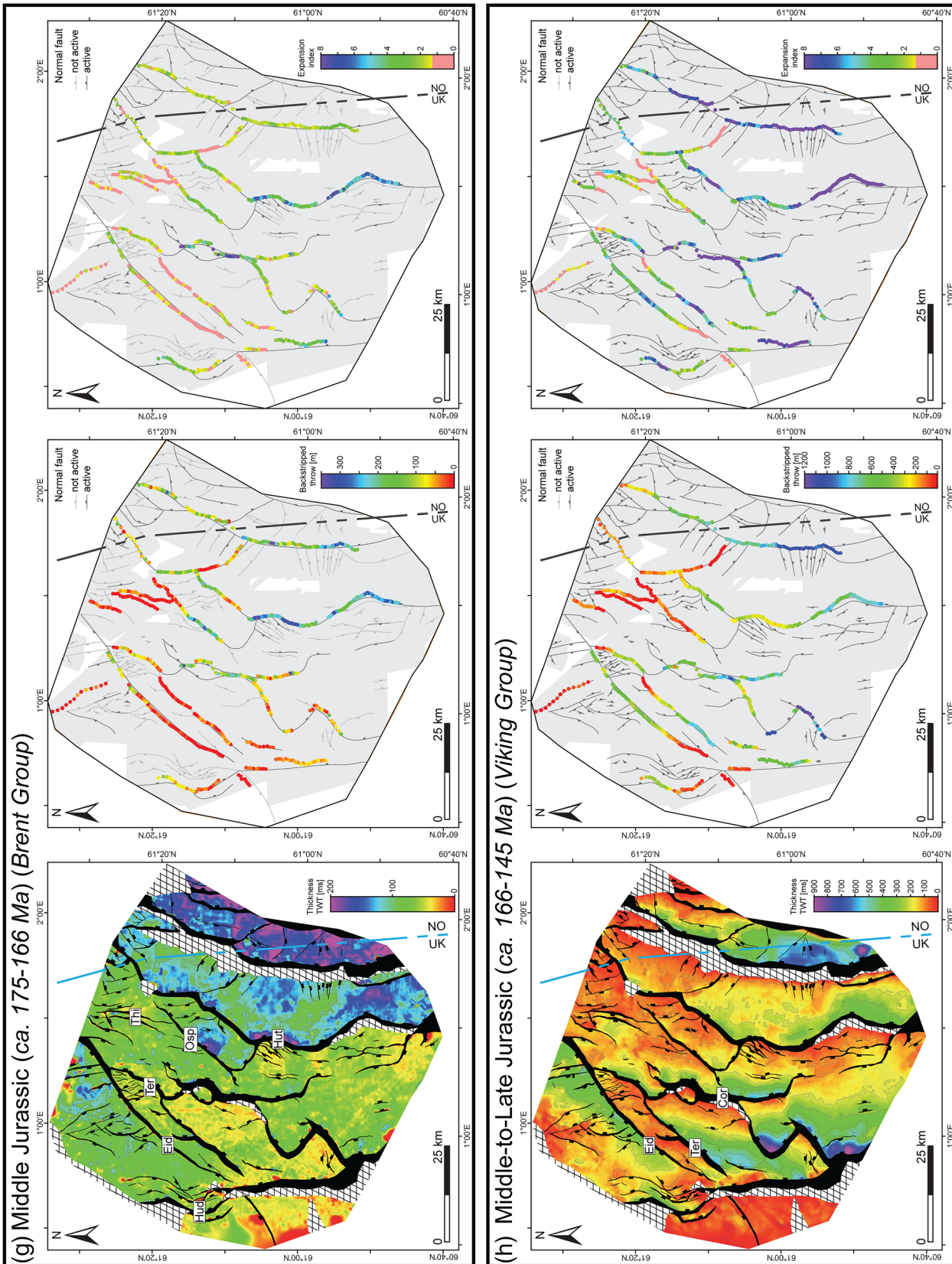


Figure 4. (Continued)

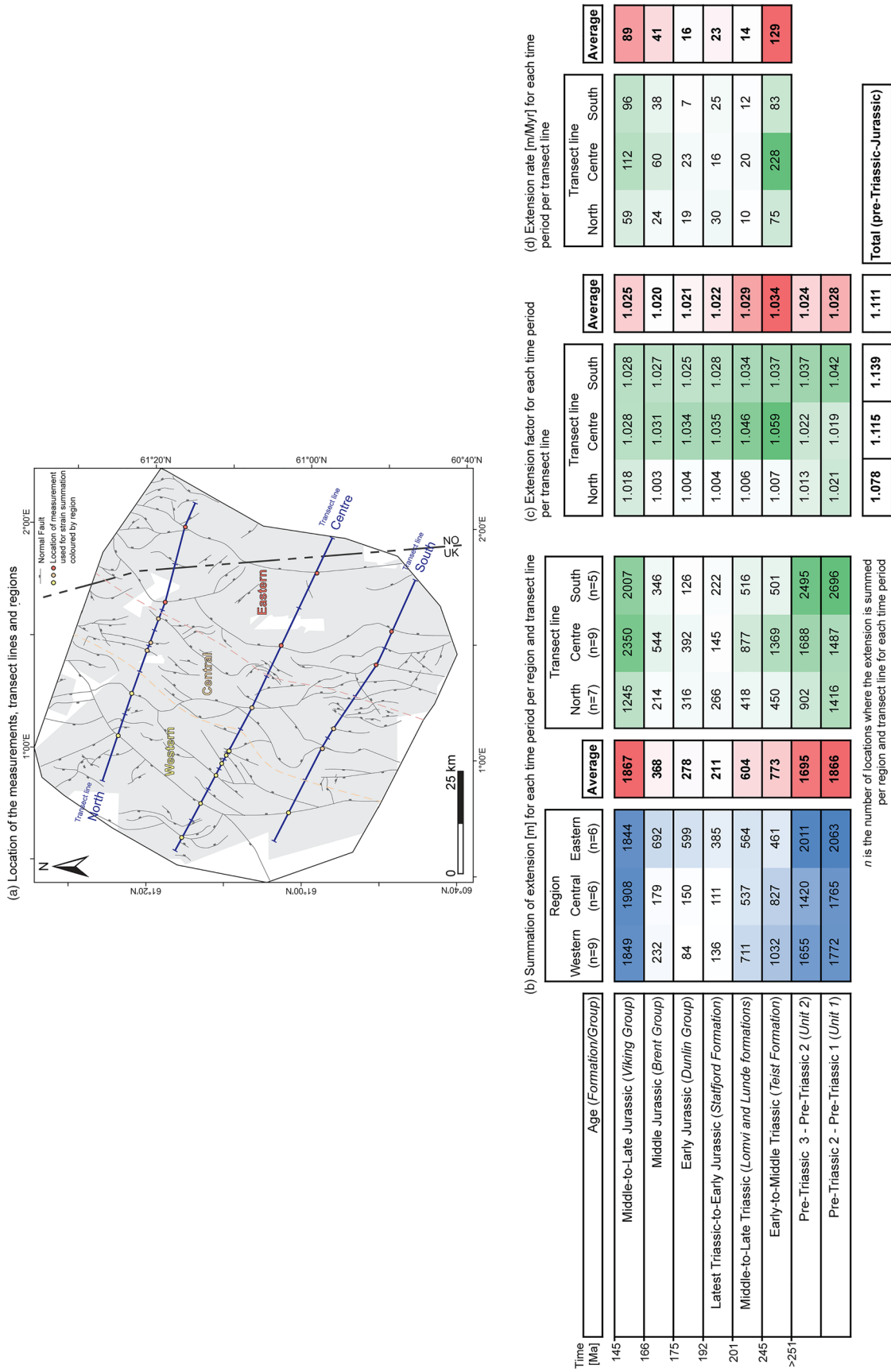


Figure 5. Strain summation across the East Shetland Basin. (a) The location of each sample location along three transect lines (north, center, and south) is shown along with the outline of the three regions (western, central, and eastern). (b) Summation of extension (m) for each time period. Values are subdivided per region, average, and transect lines. (c) Extension factor per period along each transect line and average, and total pre-Triassic-Jurassic extension factors. (d) Triassic-Jurassic extension rate (m/Myr) for each period along each transect line and average across the basin. Darker shades represent relative larger values.

Eider Fault System

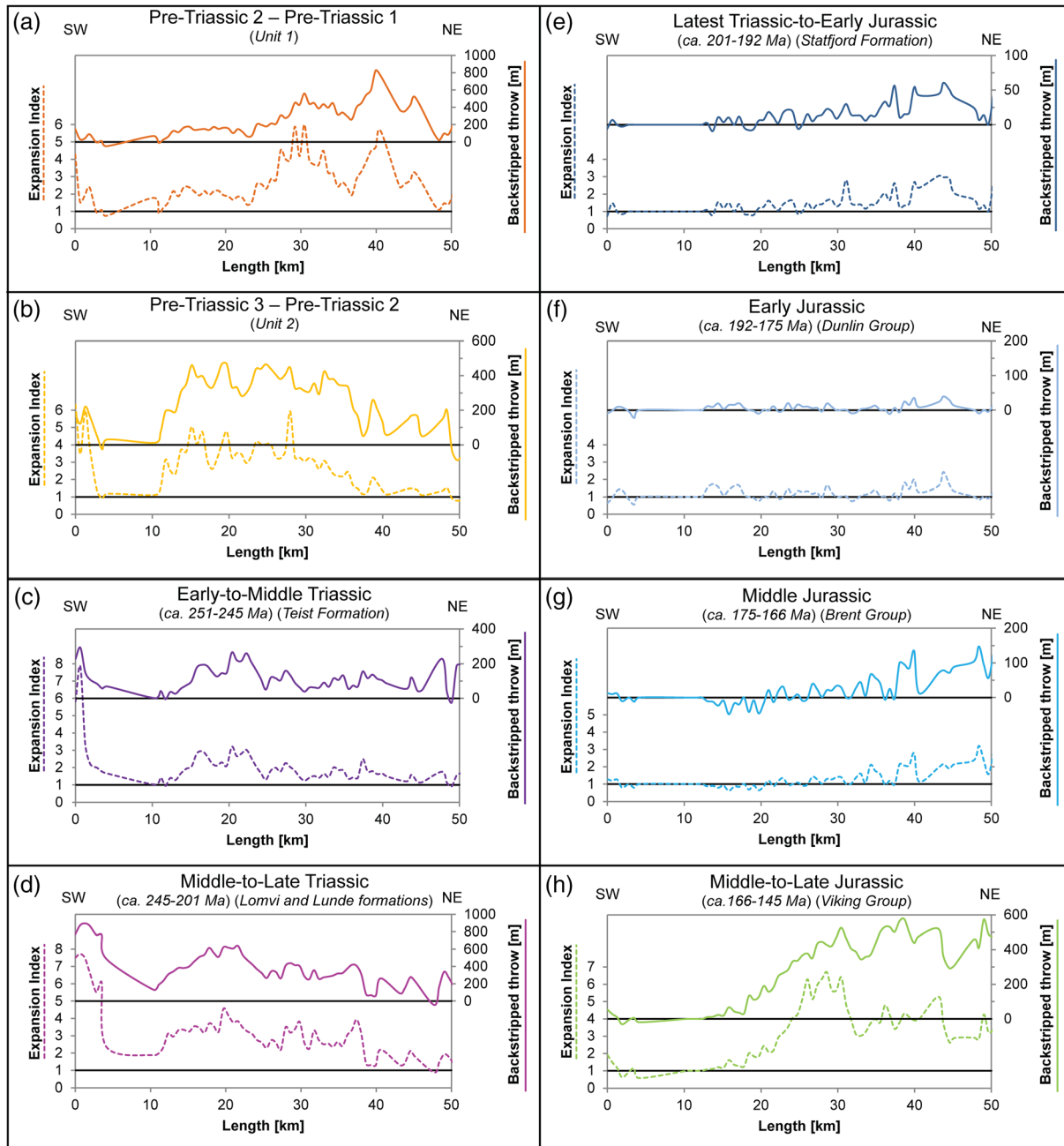


Figure 6. Expansion index (dashed) and backstripped throw (m) (continuous) along the Eider Fault System per time interval: (a) Pre-Triassic 2-Pre-Triassic 1, (b) Pre-Triassic 3-Pre-Triassic 2, (c) Early to Middle Triassic, (d) Middle to Late Triassic, (e) Latest Triassic to Early Jurassic, (f) Early Jurassic, (g) Middle Jurassic, and (h) Middle to Late Jurassic. See Figure 10 for location of Eider Fault System.

(isochrons) to determine temporal changes in accommodation related to fault slip assumes that accommodation associated with the rifting was completely filled with synkinematic deposits. In the case of underfilled basins, synkinematic deposits are limited to the hanging wall depocenter; this can result in an underestimation of the rate of accommodation generation and associated fault slip (e.g., Jackson et al., 2017). However, our data indicate that many of the fault-bound subbasins comprising the East Shetland Basin were overfilled during rifting; more specifically, seismic and, critically, well data demonstrate synkinematic deposits are preserved (and were thus deposited) in both the footwall and

Ninian-Hutton Fault System

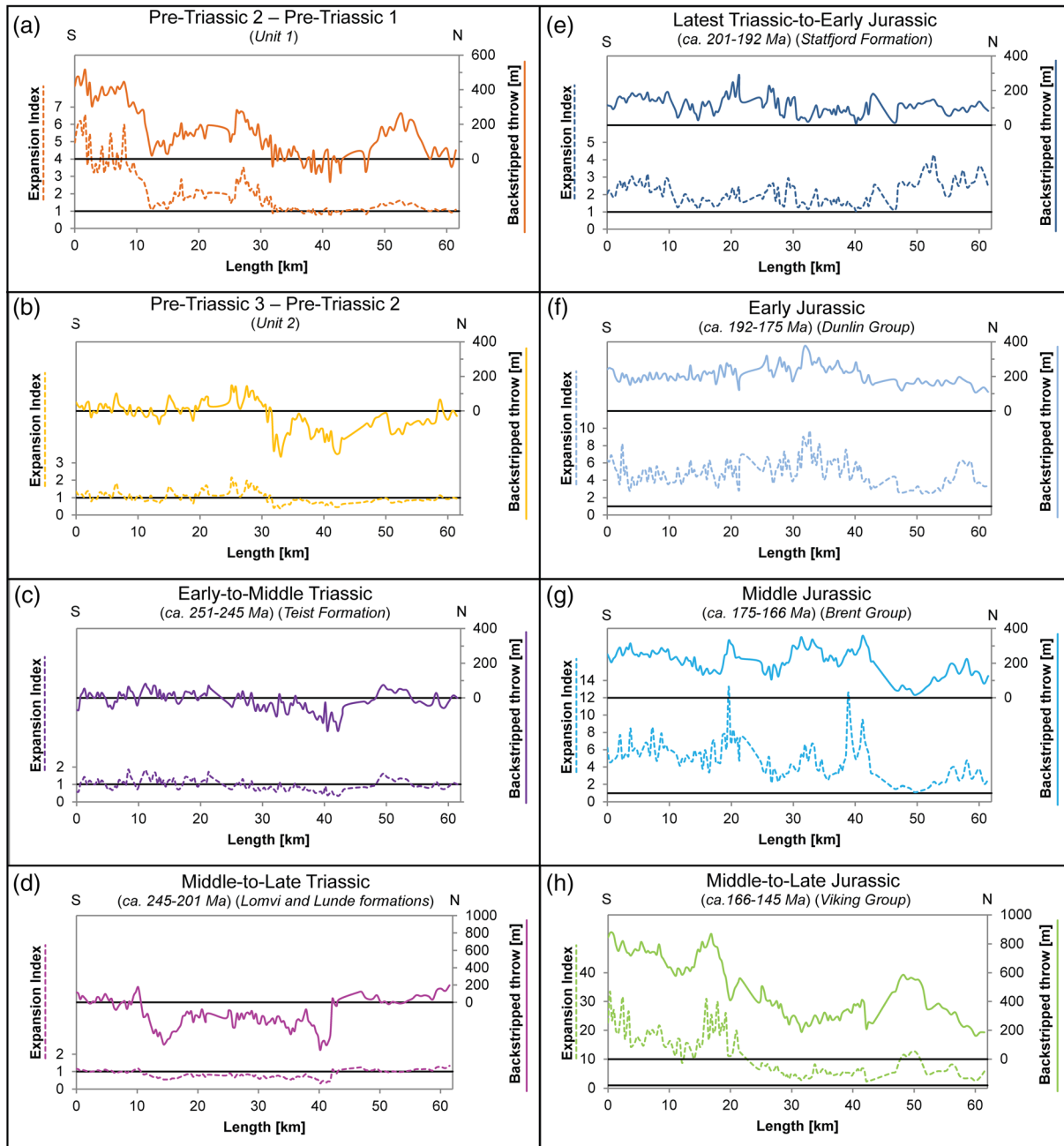


Figure 7. Expansion index (dashed) and backstripped throw (m) (continuous) along the Ninian-Hutton Fault System per time interval: (a) Pre-Triassic 2-Pre-Triassic 1, (b) Pre-Triassic 3-Pre-Triassic 2, (c) Early to Middle Triassic, (d) Middle to Late Triassic, (e) Latest Triassic to Early Jurassic, (f) Early Jurassic, (g) Middle Jurassic, and (h) Middle to Late Jurassic. See Figure 10 for location of Ninian-Hutton Fault System.

hanging walls of the faults (Figure 2). Finally, we recognize that our geometric and kinematic analysis, especially at deeper (i.e., pre-Triassic) structural levels and thus for older time periods, are likely affected by the quality of and confidence we have in our seismic interpretation and depth conversion. However, converting values from ms TWT to meters (or feet) typically preserves the spatial patterns of fault throw and does not significantly impact the related kinematic analysis (Tvedt et al., 2013). Since we focus on basin-scale trends rather than specific, absolute measurements, we consider it appropriate to use data in ms TWT, extracted directly from our time-migrated seismic data.

Cormorant Fault System

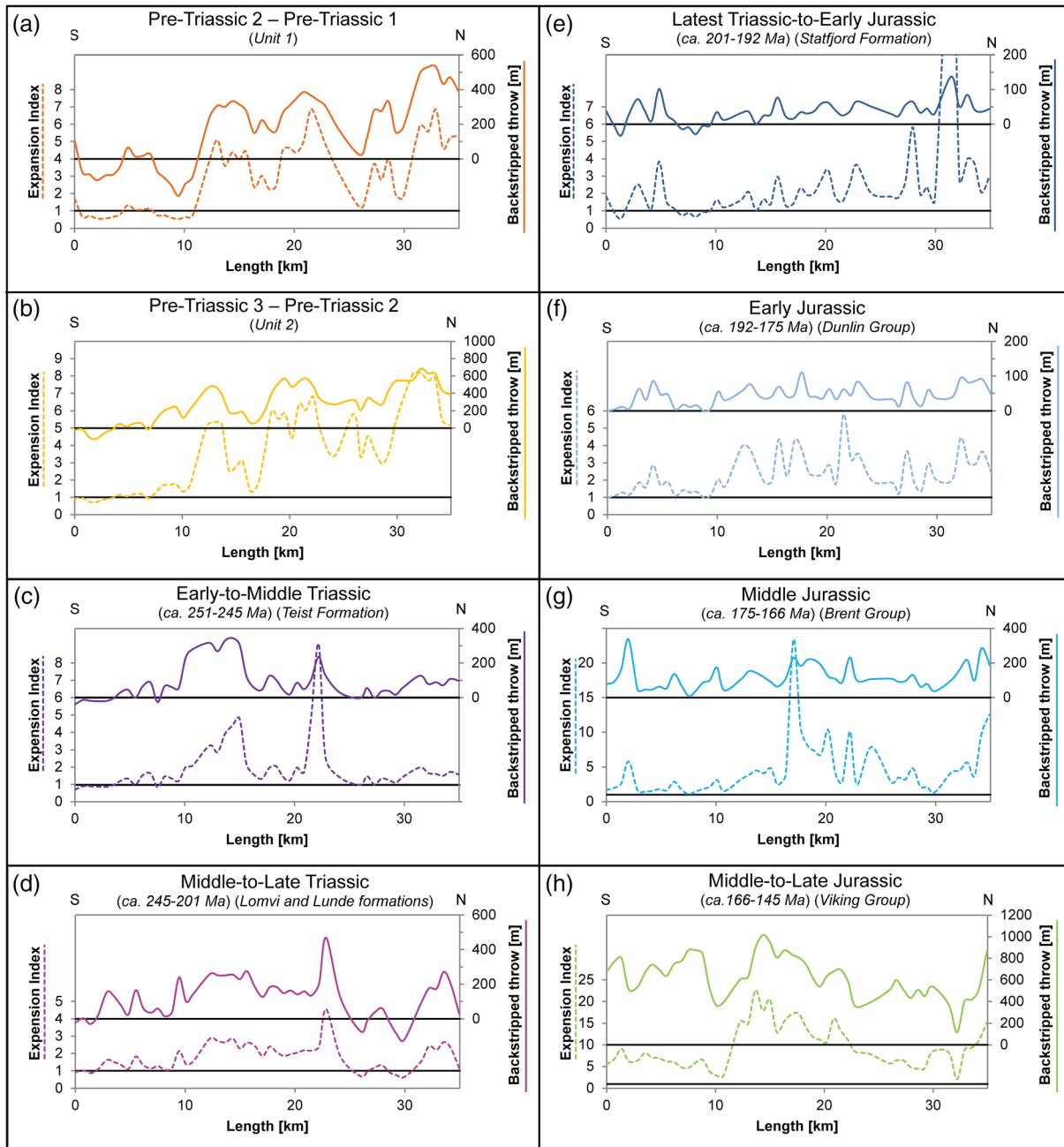


Figure 8. Expansion index (dashed) and backstripped throw [m] (continuous) along the Cormorant Fault System per time interval: (a) Pre-Triassic 2-Pre-Triassic 1, (b) Pre-Triassic 3-Pre-Triassic 2, (c) Early to Middle Triassic, (d) Middle to Late Triassic, (e) Latest Triassic to Early Jurassic, (f) Early Jurassic, (g) Middle Jurassic, and (h) Middle to Late Jurassic. See Figure 10 for location of Cormorant Fault System.

4. Spatial and Temporal Strain Variations Across the East Shetland Basin

Temporal shifts in sediment depocenters across the East Shetland Basin reflect growth of the rift-related fault array (Claringbould et al., 2017) (Figure 4). Here we reconstruct growth of major fault systems comprising the larger fault array, as well as calculating how rift-related strain varied through time at the basin scale (Figures 4 and 5).

Osprey Fault System

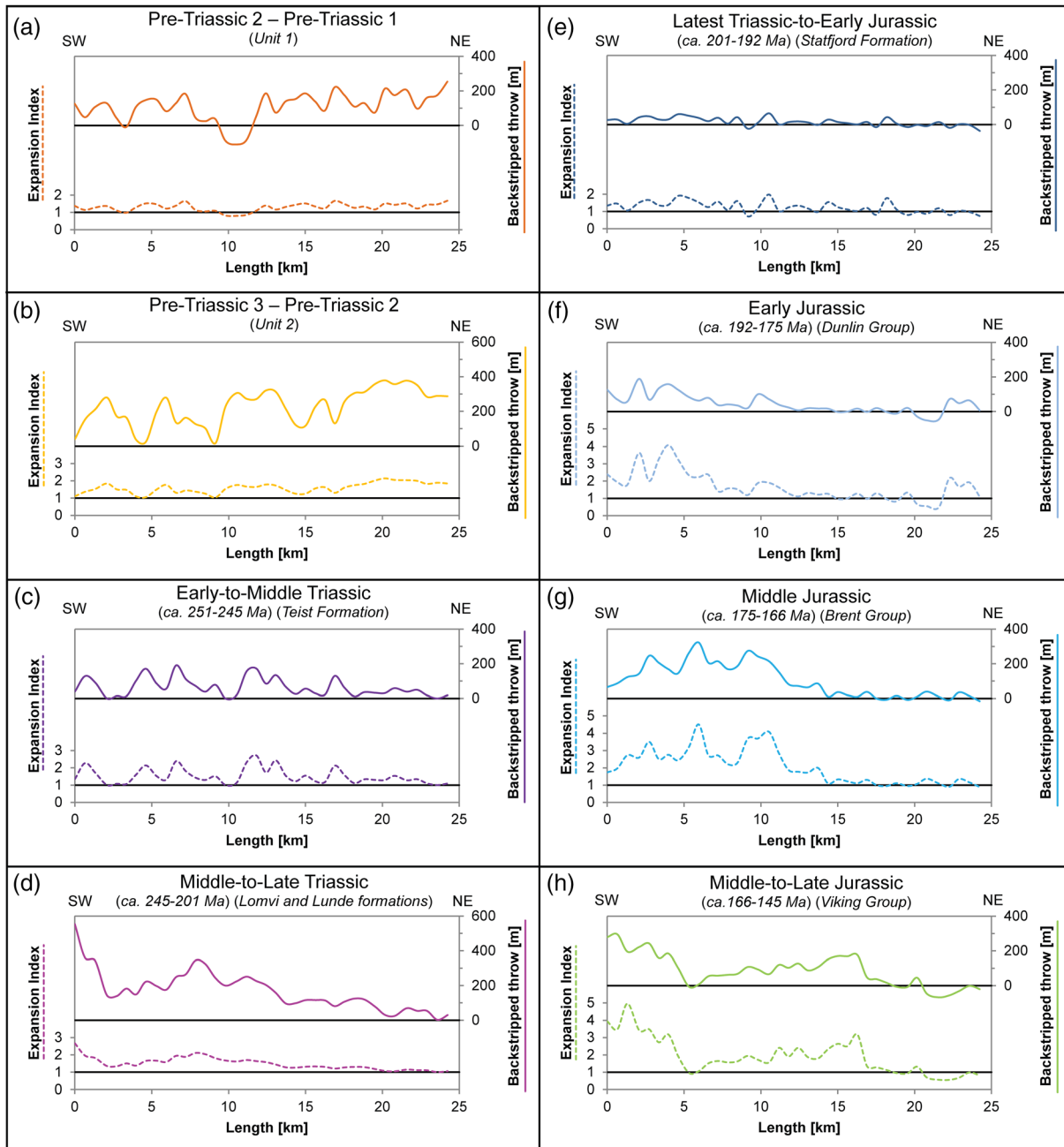


Figure 9. Expansion index (dashed) and backstripped throw [m] (continuous) along the Osprey Fault System per time interval: (a) Pre-Triassic 2-Pre-Triassic 1, (b) Pre-Triassic 3-Pre-Triassic 2, (c) Early to Middle Triassic, (d) Middle to Late Triassic, (e) Latest Triassic to Early Jurassic, (f) Early Jurassic, (g) Middle Jurassic, and (h) Middle to Late Jurassic. See Figure 10 for location of Osprey Fault System.

4.1. Pre-Triassic to Middle Triassic (>245 Ma) (Units 1 and 2, and the Teist Formation) (Figures 4a–4c)

During the deposition of pre-Triassic Units 1 and 2, and the Lower-to-Middle Triassic Teist Formation, several major fault systems in the Magnus, Tern, and Ninian Subbasins were active. These systems accumulated up to 1,200 m of throw, corresponding to large EIs of 4 to 8 (Ninian West, Heather, and Cormorant Faults, Figure 4a–4c). During the deposition of pre-Triassic Units 1 and 2, summed extension values are highest in

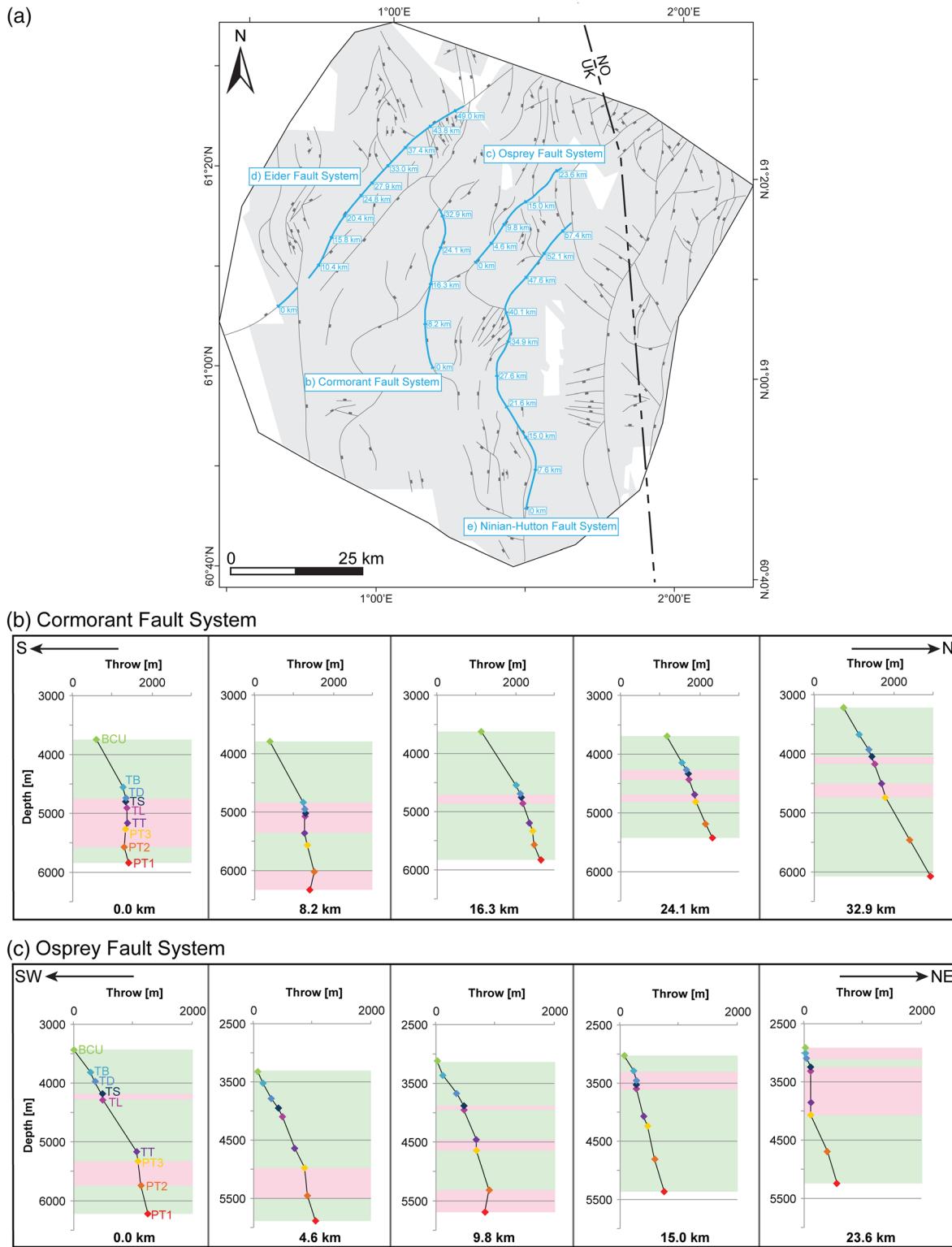
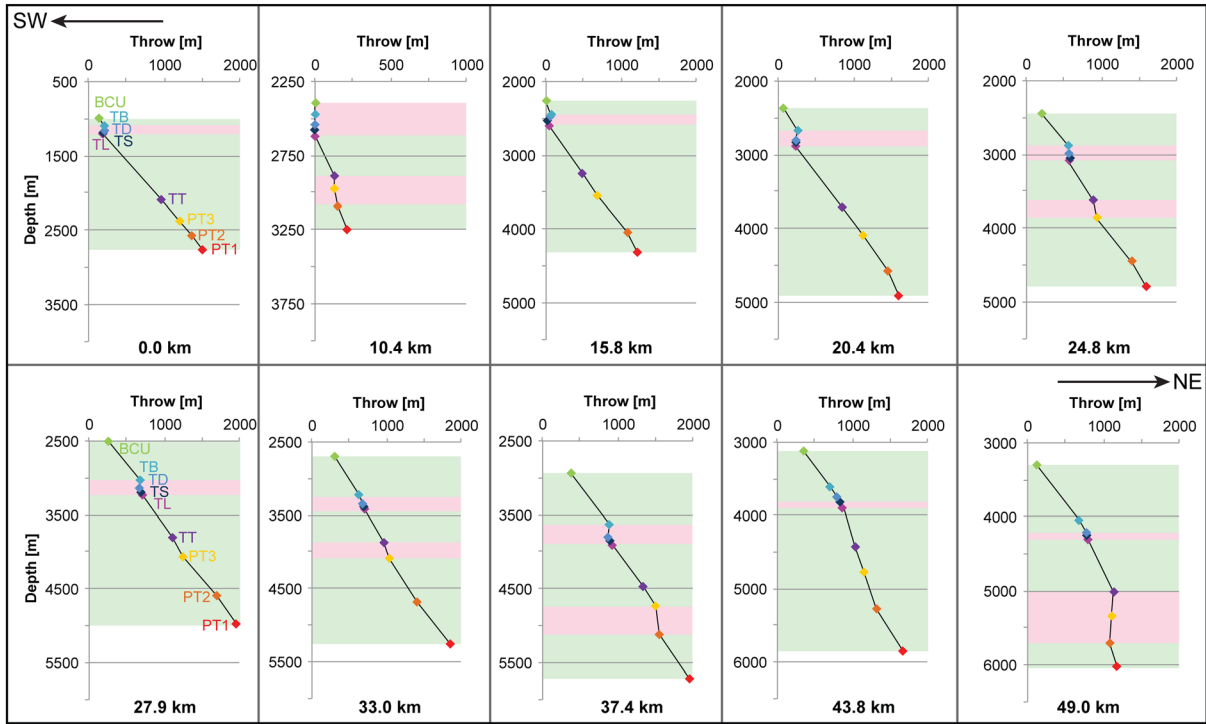


Figure 10. (a) Map of the East Shetland Basin, showing fault systems that cross the Top Brent horizon. The gray outlines the seismic data coverage. The location of the detailed analyzed fault systems are highlighted in blue with the locations of throw-depth plots marked along the length of the fault system: (b) Cormorant Fault System, (c) Osprey Fault System, (d) Eider Fault System, and (e) Ninian-Hutton Fault System. Green shaded areas are interpreted to represent fault growth activity, while red shaded areas represent inactive fault growth. BCU = Base Cretaceous Unconformity, TB = Top Brent Group, TD = Top Dunlin Group, TS = Top Stafford Formation, TL = Top Lunde and Lomvi formations, TT = Top Teist Formation, PT3 = Top Unit 2, PT2 = Top Unit 1, PT1 = Bottom Unit 1.

(d) Eider Fault System



(e) Ninian-Hutton Fault System

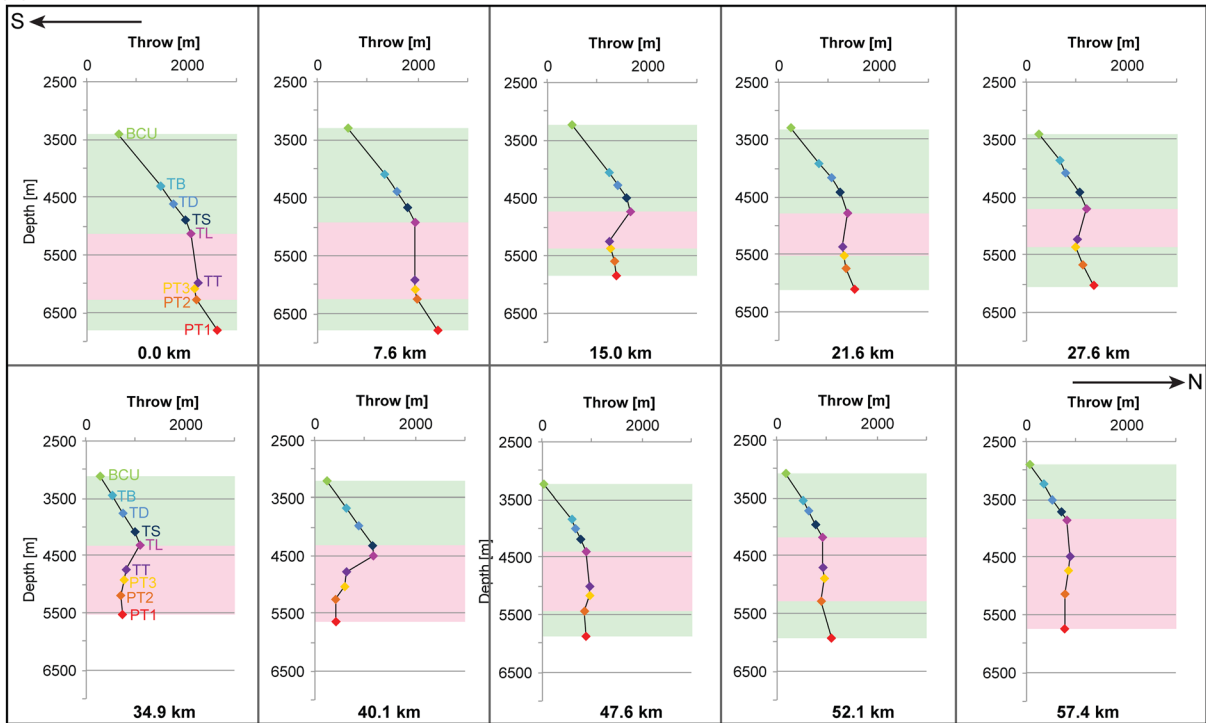


Figure 10. (Continued)

the Eastern region (up to 2,063 m) and along the southern transect (up to 2,696 m, with an extension factor of 1.042) (Figures 5b and 5c). In contrast, during deposition of the overlying Lower-to-Middle Triassic Teist Formation, most extension occurred in the western region (1,032 m) and along the central transect (1,369 m, with an extension factor of 1.059). The average extension rate in the Early to Middle Triassic was ~129 m/Myr (Figures 5b–5d). During this >50-Myr time period, extensional strain was diffuse and responsible for the formation of several subbasins.

4.2. Middle to Late Triassic (ca. 245–201 Ma) (Lunde and Lomvi Formations) (Figure 4d)

Over the next ~40 Myr, during deposition of the Middle-to-Upper Triassic Lomvi and Lunde formations, strain focused toward the southwestern part of the fault array (Figure 4d). During the early part (ca. 245–201 Ma) of the Middle Triassic-to-Middle Jurassic “interrift” period (ca. 245–166 Ma), an up to 800-m-thick sediment depocenter developed next to the southern end of the Eider Fault System, with only moderate activity (characterized by EIs <4) observed on some of the larger structures further east (Figure 4d). We calculate an average extension magnitude of 604 m for the Middle to Upper Triassic, which correlates to an average extension rate of 14 m/Myr (Figures 5b–5d); this is significantly less than that defining the previous, pre-Middle Triassic time interval (129 m/Myr) (Figure 5b).

4.3. Latest Triassic to Middle Jurassic (ca. 201–166 Ma) (Statfjord Formation, and Dunlin and Brent Groups) (Figures 4e–4g)

A significant shift in the locus of strain accumulation occurred during deposition of the uppermost Triassic-to-Lower Jurassic Statfjord Formation (Figure 4e). During this middle part (ca. 201–192 Ma) of the interrift period, moderately thick (~50 and ~250 m), relatively tabular sedimentary depocenters developed in the hanging wall of major fault systems in the eastern half of the basin (e.g., Ninian, Hutton, Alwyn, and Strathspey Fault Systems). These fault systems accumulated up to 300 m throw at this time, which was accompanied by EI value of 1.5–4 (Figure 4e). Most of this extension (385 m) accumulated in the eastern region during this time (Figure 5b), with the highest extension rate (30 m/Myr) occurring in the north of the basin (i.e., along the northern transect; Figure 5d). The average extension rate had also increased slightly from the previous time interval (from 14 to 23 m/Myr). Isochrons thus imply that strain was no longer focused on a single fault system in the western part of the basin (i.e., Eider Fault System; Figure 4d) but was now widely distributed across the eastern part of the basin, being accommodated by slip on several major fault systems.

During the latter part (ca. 192–166 Ma) of the interrift period, moderate amounts of throw (up to 300 m, associated with EIs of up to 6) accumulated on major fault systems in the east of the basin; this indicates that strain continued to be focused here for another ~25 Myr, during deposition of the relatively thin (up to 300 m) Dunlin and Brent groups (Figures 4f and 4g). Most extension occurred in the eastern region (599 and 692 m) (Figure 5b), with the largest extension factor (up to 1.034) measured along the central transect line (Figure 5c). The average extension rate initially decreased and then increased during deposition of the Dunlin (16 m/Myr) and Brent (41 m/Myr) groups in the Early to Middle Jurassic (cf. 23 m/Myr during the Early Jurassic; Figure 5d).

4.4. Middle to Late Jurassic (ca. 166–145 Ma) (Viking Group) (Figure 4h)

In contrast to the interrift period (ca. 192–166 Ma), when strain was relatively focused in the east of the East Shetland Basin, strain is distributed across the whole basin during deposition of the Middle-to-Upper Jurassic Viking Group (Figure 4h). Up to 1,200 m of throw accumulated on the major fault systems across the East Shetland Basin, forming thick (up to 900 m) depocenters that were associated with high EIs (6–8) (Figure 4h). Extension was distributed relatively evenly across the Western, Central, and Eastern regions in the basin (1,849, 1,908, and 1,844 m, respectively) (Figure 5b). We observe an increase in both strain accumulation and extension magnitude in the East Shetland Basin compared to the Early Jurassic. First, EI values that are locally <4 during the deposition of the Lower Jurassic Dunlin Group (Figure 4f), increase to 6–8 across much of the basin during deposition of the Middle-to-Upper Jurassic Viking Group (Figure 4h). Second, the average extension factor (1.025 compared to 1.021) and extension rate (89 compared to 16 m/Myr) are both significantly higher during the Middle to Late Jurassic compared to the Early Jurassic (Figures 4f–4h, 5c, and 5d).

4.5. Early Cretaceous (ca. 145–140 Ma) (Cromer Knoll Group)

In this study we did not focus on the Early Cretaceous phase of extension in the East Shetland Basin. However, several studies show that during the earliest Cretaceous (ca. 140–145 Ma; i.e., Valanginian-Berriasian), active faulting migrated eastward onto the fault systems separating the East Shetland Basin from the deep rift axis of the North Viking Graben (so-called “Visund-Gullfaks fault” of Cowie et al., 2005; see also Færseth et al., 1995; McLeod et al., 2002; Phillips et al., 2019). Strain localization onto these structures, which lie just east of the area imaged by our seismic reflection data (see Figure 1), was associated with overall rift narrowing (from >200 m to ~50 km) and ultimately abandonment of the East Shetland Basin (Cowie et al., 2005). To the best of our knowledge, extension factor and magnitude have not been calculated for this specific period of late synrift strain localization. However, subsidence inversion (Newman & White, 1999) and geological observations (Cowie et al., 2005) suggest that strain rate declined rapidly (from 3×10^{-16} to $3 \times 10^{-17} \text{ s}^{-1}$) from the Late Jurassic into the Early Cretaceous. Final abandonment of the North Viking Graben (and the northern North Sea rift system in general) occurred later in the Cretaceous (Phillips et al., 2019).

5. Relationship Between Fault System and Fault Array Growth

During deposition of pre-Triassic and earliest Triassic, strain was distributed across the basin, with most strain accommodated along the south transect line (see section 4.1). With the exception of the Osprey Fault System (Figures 9a–9c), which was located in the center of the basin (Figure 10), the presence of multiple throw and EI maxima along all major fault systems during deposition of Unit 1 suggest these structures grew by the growth and linkage of initially isolated fault segments (Figures 6a–6c and 8a–8c). Postlinkage, strain could have migrated along strike, as illustrated by the Eider Fault System, which saw an overall south-westward migration of activity through time (Figures 6a–6c).

During the early part (ca. 245–201 Ma) of the interrift period, strain was primarily focused in the western region, along the Eider Fault System. At the southwestern tip of the Eider Fault System, up to 900-m throw accumulated at this time, decreasing to ~200 m along strike toward the northeastern fault tip (Figure 6d). Relatively little strain was accommodated along the Cormorant and Osprey Fault Systems in the basin center at this time (<500-m throw), with only some small segments of these structures being active (Figures 8d and 9d). The Ninian-Hutton Fault System, which was located in the eastern part of the basin, was inactive (Figure 7d; see also T-z plots in Figures 10b, 10c, and 10e). We also observe an overall decrease in slip rate from the previous, pre-Middle Triassic time interval (from a maximum of ~100 to ~25 m/Myr) (Figures 11a and 11b); however, because the age of the lower boundary of the Teist Formation is poorly constrained, these rates could be overestimated.

During the middle and latter part (ca. 201–166 Ma) of the interrift period, strain migrated from the western to eastern part of the basin. With the exception of its northeastern tip, the Eider Fault System was largely inactive, illustrated by vertical intervals on the corresponding T-z plots (Figure 10d). Strain was distributed relatively evenly along the length of the Cormorant, Osprey, and Ninian-Hutton Fault Systems during deposition of the Statfjord Formation (Figures 7e and 9e). Latest Triassic-to-Middle Jurassic slip rates increase from 20–30 m/Myr during deposition of the Statfjord Formation (Figure 11c) to 25–75 m/Myr during deposition of the Brent Group (Figures 11d and 11e). Reactivation of the Ninian-Hutton Fault System during deposition of the Statfjord Formation is clearly captured in the T-z plots. For example, between Pre-Triassic 1 and 2, activity occurred along two segments (i.e., 0 to ~30 km and ~45 to ~55 km; Figure 10e). Periods of fault inactivity along the entire length of the Ninian-Hutton fault are marked on T-z plots by vertical intervals, the tops of which defined by the Top Lunde horizon; above this, throw decreases, indicating fault reactivation (Figure 10e).

During the Middle to Late Jurassic, strain was distributed across the basin and accommodated by relatively rapid slip (up to 100 m/Myr; cf. Cowie et al., 2005) on many of the major fault systems (Figure 11). However, a key observation is that strain was not distributed evenly along these fault systems. For example, local throw minima that are associated with and thus define the position of now-breached relays, and which were inherited from earlier, possibly even pre-Triassic stage of rifting and fault linkage, persisted (Figure 6h).

Lastly, during the Early Cretaceous, strain focused on the Visund-Gullfaks fault (Figure 1) as the rift narrowed (Cowie et al., 2005; McLeod et al., 2002). Despite an overall decrease in strain rate (Newman &

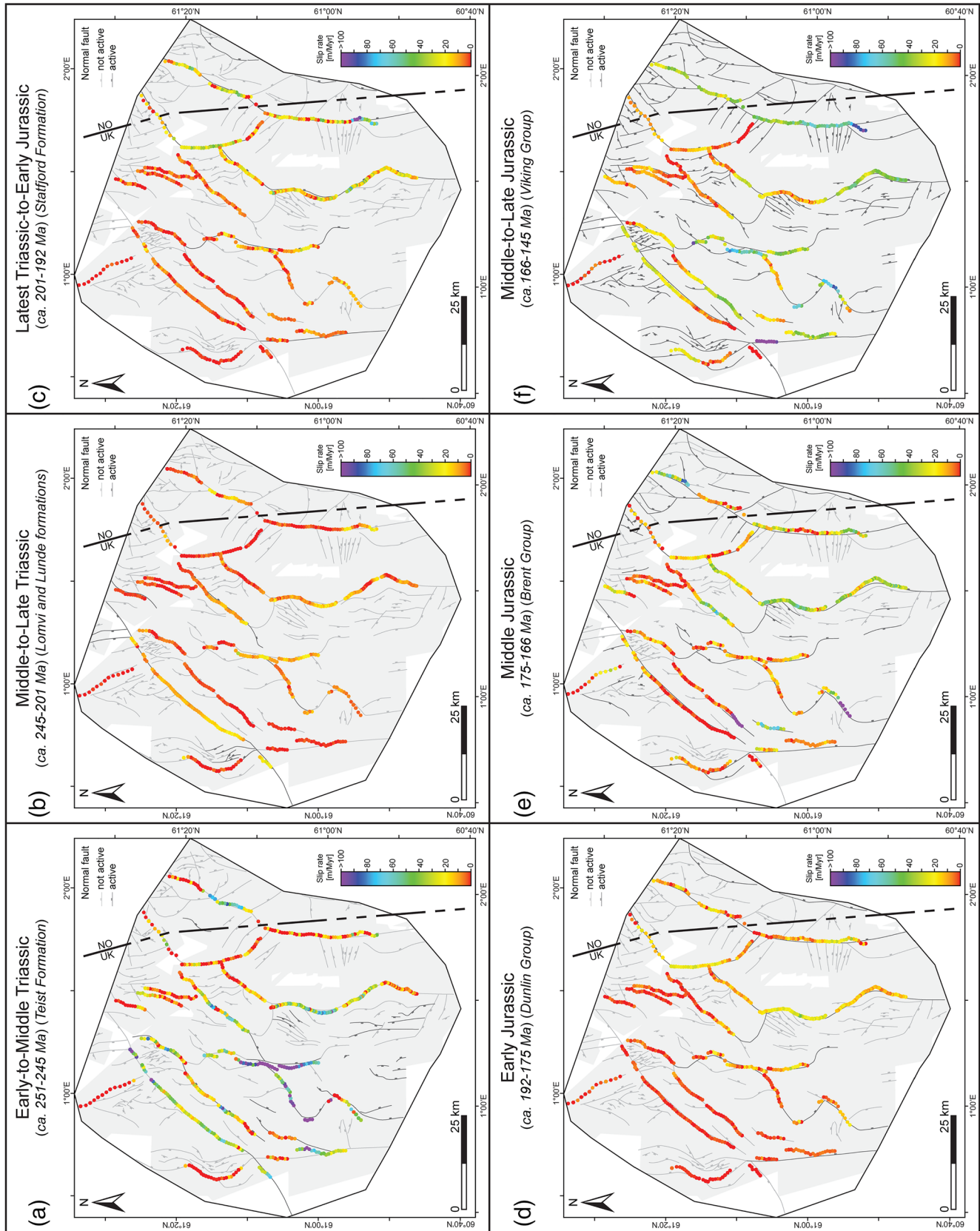


Figure 11. Line drawing of faults over outline of 3-D seismic data coverage (gray polygons) overlain by Triassic-Jurassic fault slip rates across the East Shetland Basin per time interval: (a) Early to Middle Triassic, (b) Middle to Late Triassic, (c) Latest Triassic to Early Jurassic, (d) Early Jurassic, (e) Middle Jurassic, and (f) Middle to Late Jurassic.

White, 1999), maximum slip rates on the Visund-Gullfaks fault were apparently the highest that had ever occurred in the East Shetland Basin (~300 m/Myr) (Cowie et al., 2005).

6. Discussion

6.1. Temporal and Spatial Changes in the Basin-Scale Distribution of Rift-Related Strain

Despite rifting being rather protracted (~150 Myr), the northern North Sea region experienced only the early phases of continental rifting (i.e., the *stretching* and the onset of the *thinning phase* of Péron-Pinvidic et al., 2013); full plate rupture was not achieved. The East Shetland Basin forms part of the so-called proximal domain; this is a domain characterized by classical graben and half-graben basins filled with wedge-shaped, syntectonic sedimentary units mainly deposited during the initial stretching phase (Péron-Pinvidic et al., 2013). We propose that rift-related strain was partitioned in different parts of the basin and migrated through time. Figure 12 illustrates the qualitative strain distribution across the fault array in the East Shetland Basin from the pre-Triassic to Late Jurassic, based on our detailed, quantitative fault array analyses. Spatial variations in the timing and magnitude of slip occurred along strike of major fault systems that make up the larger host fault array. This reflects the heterogeneous nature of the early rift-related strain within the East Shetland Basin (Figure 12).

Strain migration along individual fault systems is common, typically reflecting fault growth by segment linkage, rheological differences in the deforming host rock, and/or the presence of preexisting structures (e.g., Cowie et al., 2000; Duffy et al., 2015; Jackson et al., 2017; McLeod et al., 2000, 2002; Nixon et al., 2014; Putz-Perrier & Sanderson, 2008; Soliva et al., 2006; Tomasso et al., 2008; Walsh et al., 2003; Whipp et al., 2014; Young et al., 2001). Segment linkage and preexisting structures played a role in the growth of several fault systems (e.g., segment linkage at Eider Fault System, Figures 6a and 6b; see also McLeod et al., 2002). However, we see no clear evidence that preexisting structures dictated temporal variations in rift-related strain in the East Shetland Basin. This observation is consistent with Claringbould et al. (2017) and Cowie et al. (2005), who both propose that strain accumulation patterns during growth of upper crustal normal fault systems, even during the relatively early stages of continental rifting, are controlled by the thermal and mechanical state of the entire lithosphere.

Complex strain migration patterns during the early phases of continental rifting, such as those identified in the East Shetland Basin, could be caused by the emplacement of magmatic bodies (e.g., Buck, 2006; Corti et al., 2003; Stab et al., 2016; Wolfenden et al., 2005). However, in the East Shetland Basin we see no clear evidence for significant rift-related magmatism, suggesting the emplacement of igneous bodies did not control how rift-related strain accumulated. Other studies link strain migration to flexural downbending of the crust (e.g., Bayona & Thomas, 2003; Bell et al., 2014). Indeed, on the eastern margin of the northern North Sea, Bell et al. (2014) observe that the strain migrates away from the Middle-to-Early Cretaceous rift axis (North Viking Graben, Figure 1a), after a phase of Permian-Triassic rifting and Early Jurassic tectonic quiescence. However, flexural downbending of the upper crust is typified by the overall migration of strain either toward or away from the principle rift axis, making it unlikely that this is the cause for the far more complex patterns observed in the East Shetland Basin (Figure 12). Cowie et al. (2005) show that Middle-to-Early Cretaceous rift-related strain in the East Shetland Basin migrated toward the rift axis during the rift maximum, relating this to a change in the geometry of the underlying thermal perturbation associated with the initial phase of rift narrowing (i.e., an increase of vertical thermal gradient toward the rift axis; e.g., Behn et al., 2002; Huismans et al., 2001; Nagel & Buck, 2007). However, their study is spatially restricted to the eastern part of the East Shetland Basin and considered only Middle-to-Early Cretaceous rifting. By considering the entire basin, which essentially represents the entire western margin of the northern North Sea rift system, and the full, ~150-Myr duration of rift activity, we show a much more complicated history comprising temporal and spatial changes in both strain distribution (Figure 12), and extension magnitude and rate (Figures 4, 5d, and 11). Our study thus highlights that a full understanding of the early stages of continental breakup requires analysis of a sufficiently large study area (at least one margin of the rift system) and needs to consider a sufficiently long period of rift development.

6.2. Variation in Extension Magnitude and Rate During Rifting

We show that extension magnitudes and rates in the East Shetland Basin vary in space and time (Figure 5). For example, extension and fault slip rates decrease and stay relatively low (≤ 30 m/Myr) for ~70 Myr during

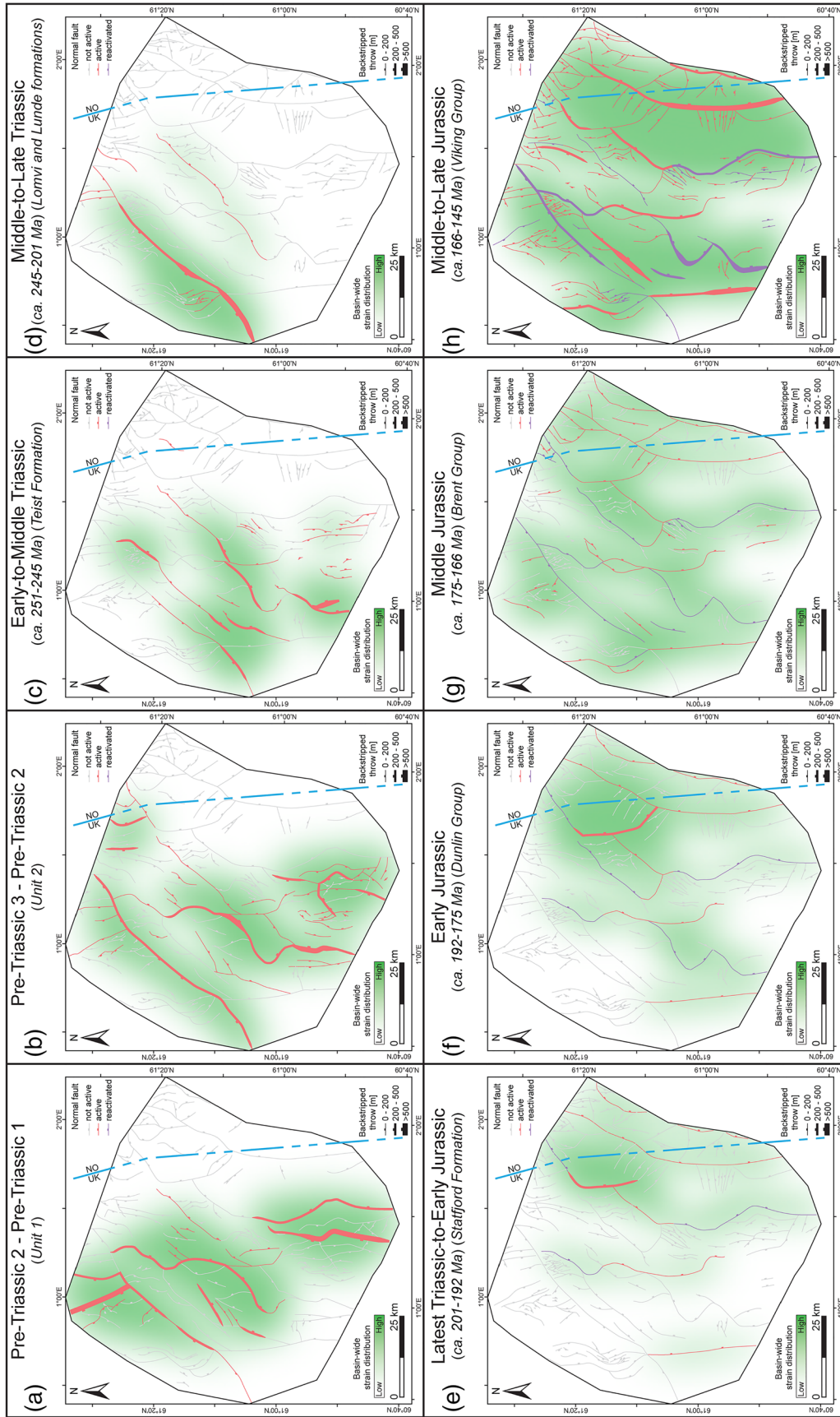


Figure 12. Basin-wide strain distribution across the East Shetland Basin per time interval: (a) Pre-Triassic 2-Pre-Triassic 1, (b) Pre-Triassic 3-Pre-Triassic 2, (c) Early to Middle Triassic, (d) Middle to Late Triassic, (e) Latest Triassic to Early Jurassic, (f) Early Jurassic, (g) Middle Jurassic, and (h) Middle to Late Jurassic.

the Middle Triassic-to-Middle Jurassic interrift period (Figures 5d and 11a–11c). From the Middle Jurassic onward, slip rates increase for ~ 30 Myr (Figure 5d) to ≥ 50 m/Myr (Figures 11d–11f). Maximum slip rates of ~ 300 m/Myr eventually occur during the Early Cretaceous on very large fault systems bounding the East Shetland Basin (Cowie et al., 2005).

We propose that changing extension rates may account for the strain distribution trends we observe, consistent with the predictions of lithospheric-scale numerical models (e.g., Bassi, 1995; Brune et al., 2016; England, 1983; Houseman & England, 1986; Kusznr & Park, 1987; Naliboff & Buitter, 2015; Naliboff et al., 2017; Péron-Pinvidic et al., 2013; Van Wijk & Cloetingh, 2002). The distributed faulting that defined the pre-Triassic period (Figures 12a–12c) may reflect the relatively slow, pre-Jurassic extension rates. This is consistent with the 2-D lithosphere-scale numerical modeling results of Naliboff et al. (2017), who suggest that a relatively slow ($< 5,000$ m/Myr) extension rate during the initial stage of rifting is associated with uniform lithospheric thinning and distributed upper crustal faulting. Subsequently, Triassic strain focused on a small number of fault systems, while elsewhere in the basin minimal to no fault growth activity took place for ~ 45 Myr. We suggest that, during this interrift period, the relatively slow and decreasing extension rate induced local synrift cooling and was associated with limited fault activity (Figures 5d, 11c, 12d, and 12e) (e.g., Bassi, 1995; England, 1983; Kusznr & Park, 1987; Naliboff & Buitter, 2015; Van Wijk & Cloetingh, 2002). This interpretation is consistent with the predictions of previous 2-D lithospheric-scale models (e.g., Naliboff et al., 2017; Van Wijk & Cloetingh, 2002). Van Wijk and Cloetingh (2002) model synrift cooling in a region that initially extended at a relatively slow rate ($< 8,000$ m/Myr). Subsequently, a shift in the locus of maximum extension occurs: the “old” rifted subbasin is abandoned, and extension concentrates in other areas of the larger rift system. Van Wijk and Cloetingh (2002) compare their modeling results to several continental margins, including the Mid-Norwegian Margin, which is of comparable size and has a similar extension history to the East Shetland Basin. They find that strain migration patterns between their slow extension rate models ($< 8,000$ m/Myr) and natural example are similar; that is, the gap between successive rifting events, during which time the locus of strain migrates, is of a similar magnitude (~ 20 – 60 Myr).

In contrast to initially slow and decreasing extension rates, we suggest that immediately post-Triassic patterns of faulting in the East Shetland Basin are controlled by the increasing rate of lithospheric extension (Figure 5d). We propose that eastward migration of strain during the latest-Triassic to Early Jurassic reflect the initial phase of lithospheric necking and rift narrowing (e.g., Behn et al., 2002; Cowie et al., 2005; Huismans et al., 2001; Nagel & Buck, 2007; Péron-Pinvidic et al., 2013) (Figures 12e and 12f). The main Middle Jurassic-to-Early Cretaceous rift phase is ultimately characterized by the highest extension and fault slip rates (Figures 5d and 11f). This phase of rifting is also defined by distributed faulting, which involves the reactivation of some pre-Jurassic faults, as well as the growth of new faults (Figure 12h). Our observations are consistent with the numerical model predictions of Naliboff et al. (2017) who show that when extension rate increases ($> 5,000$ m/Myr), strain localizes near a heated and weakened rift axis as the advective heating of the lithosphere exceeds the conductive cooling; this can drive rift narrowing. Naliboff et al. (2017) also predict that when the extension rate increases after an initial period of relatively slow extension ($< 5,000$ m/Myr), the upper crustal rift pattern is characterized by the growth of new faults and the reactivation of the earlier developed, more widely distributed normal faults. Corti et al. (2013) also show that a relatively high rate of extension is associated with an overall inward migration of faulting toward the rift axis. However, their lithosphere-scale, centrifuge sand-box experiments imply that inward migration of faults during rifting are also subject to other factors such as the thickness of brittle and ductile layers, the width of the weak zone that localizes extension, and the degree of rift obliquity (Corti et al., 2013).

6.3. Comparing Extension Magnitudes and Rates in Relation to Rift Pattern Evolution

Depending on which numerical models is used, the absolute velocity threshold for which synrift cooling will or will not occur ranges between 1,500 and 8,000 m/Myr, (e.g., Bassi, 1995; Naliboff et al., 2017; Van Wijk & Cloetingh, 2002). This likely reflects variations in the initial conditions used by the different models, given that Bassi (1995) shows that this transition velocity is highly dependent on the rheology of the rifted lithosphere (see also Bassi, 1991; Buck, 1991). It is therefore difficult to directly compare different models or natural rift systems, or models to natural examples.

We note, however, a marked discrepancy between the extension rates we calculate in the East Shetland Basin (10–225 m/Myr) and those determined in active rift systems by geodetic data (e.g., 4,000 m/Myr,

Main Ethiopian Rift, Bendick et al., 2006; 4,500 m/Myr, Baikal Rift, Calais et al., 1998; 15,000 m/Myr, Red Sea Rift, McClusky et al., 2010). This discrepancy likely reflects several factors that control the rate of plate stretching, as well as the resolving powers of the various analytical tools. First, we note that the extension rates quoted above are for the full rift width, whereas we only consider approximately a third of the width of the northern North Sea rift system. Most critically, as the East Shetland Basin is limited to the western margin of the larger rift system, our analysis is outside of the main rift axis (i.e., the North Viking Graben, within which most of the Pre-Triassic-to-Jurassic extension took place; e.g., Odinsen et al., 2000) (Figure 1a). Additional minor causes for the discrepancy may reflect the fact we are unable to calculate the true magnitude of upper crustal extension (and thus extension rate) using a relatively low spatial-resolution tool like seismic reflection data. Walsh and Watterson (1992) note that the fractal distribution of fault sizes mean that up to 30% of extension can be taken up along subseismic faults (i.e., faults that are smaller than the seismic resolution).

However, when comparing our extension factors with those presented previously from the northern North Sea, a discrepancy is less apparent. Roberts et al. (1993, 1995) use tectonostratigraphic forward models to calculate the extension factor across the East Shetland Basin for the Permian-Triassic (1.15) and Jurassic (1.15) rift phases. Using a similar method, Odinsen et al. (2000) suggest slightly different values (i.e., 1.29 and 1.11 for the Permian-Triassic and Jurassic phases, respectively). However, in contrast to these and other workers, we argue for a single, protracted phase of rifting; that is, we do not identify two, discrete periods of rifting separated by a phase of tectonic quiescence. For the entire Pre-Triassic-to-Jurassic period, we calculate an average extension factor of 1.11 along three transects across the East Shetland Basin (Figure 5c). This slight difference between our extension factors and those previously calculated (i.e., Odinsen et al., 2000 and Roberts et al., 1993, 1995) likely arises due to the different time intervals considered and the different extents and locations of the fault normal transects used to calculate the extension factors.

6.4. Extension Rate Variability During Rifting

Despite the absolute discrepancy between our and previously observed and predicted extension and strain rates (section 6.3), our results are qualitatively consistent with the predicted effect of changes in extension and strain rates on the rift pattern evolution (e.g., Bassi, 1995; Naliboff et al., 2017; Van Wijk & Cloetingh, 2002). We show that extension rate decreases during the Triassic and increases throughout the Jurassic in the East Shetland Basin (Figure 5d). We suggest that these changes are responsible for the observed patterns of rift-related faulting and overall rift geometry (Figure 12). Although difference in lithospheric characteristics between natural rift systems (e.g., rheology) complicate a direct comparison of extension rates, and its resultant effect on rift geometry, changes in relative extension rate during rifting have been observed in natural rift systems elsewhere (e.g., Brune et al., 2016; Ford et al., 2013). Based on plate reconstructions, Brune et al. (2016), show that an abrupt acceleration in extension rate ~ 10 Myr before breakup is apparent in the South Atlantic, central North Atlantic, North America-Iberia, and Australia-Antarctica rifts, as well as during opening of the and South China Sea. Brune et al. (2016) argue that this is the result of dynamic rift weakening; that is, as long as the rift is strong, the extension rate is low, but with continued deformation the rift axis weakens, and extension accelerates due to crustal necking and strain softening. Ford et al. (2013) use field data to calculate a significant increase in extension rates during the development of the young (< 5 Myr), still-active Corinth Rift, whereas Nixon et al. (2016) use field and subsurface data to illustrate a relatively rapid (i.e., over a 300-kyr period) transition from a structurally complex, northward migrating rift to a predominantly asymmetric rift. They argue that this rapid change in rift structure over a relatively short period of extension can reflect multiple parameters, including an increase in extension rate (Corti et al., 2013).

Our results suggest that relative changes in extension rate play an important role in the basin-wide strain behavior we observe in the East Shetland Basin (and the northern North Sea in general) during pre-Triassic-to-Late Jurassic rifting. We propose that lack of a clear direction for strain migration, especially during pre-Jurassic extension, shows that the early stages of continental rifting is complex due to a range of an underlying controlling factors such as variation in extension rate, evolving geometry of underlying thermal perturbation, and the influence of faults developed during the initial stage of rifting. It is possible that the limited spatial and temporal dimensions used by the previous studies in the northern North Sea meant details of this heterogeneous strain distribution and complex rift pattern evolution were missed (e.g., Badley

et al., 1988; Bell et al., 2014; Cowie et al., 2005; Færseth, 1996; Lee & Hwang, 1993; Odinsen et al., 2000; Roberts et al., 1993, 1995; Thomas & Coward, 1995; Tomasso et al., 2008). Therefore, high-resolution observations and analyses across at least a fault array, and over a considerable period of the rift event, are necessary to fully resolve the dynamics of continental rift development. Moreover, these details of three-dimensional strain behavior during rift-related extension and its effect on the rift pattern evolution should be considered in future numerical and physical models.

7. Conclusions

Using an extensive, high-resolution subsurface data set, we observe complex strain partitioning and varying extension rates during the ~150-Myr rift development of the East Shetland Basin, northern North Sea. Comprehensive quantitative fault growth analyses across the entire width of the basin enable us to document the development of a fault array on one margin of a failed rift system and analyze the related strain accumulation pattern over time (Figure 12). Our results highlight the complicated three-dimensional behavior of strain in the upper crust during the early stages of continental rifting.

For extended periods of time (>20 Myr) we find that strain is distributed across the full width of the basin where it accumulates and localizes at different parts, while during other time intervals we observe minimal to no fault growth (Figure 12). Furthermore, we calculate varying extension magnitudes and rates across the basin over time. Average extension factor ranges between 1.020 and 1.034, and average extension rates range between 14 and 129 m/Myr (Figures 5c and 5d). This variation marks different time intervals of relatively low and high rift activity during rifting in the East Shetland Basin. Fault segment linkage and prior rift structures affect the localization of strain within major fault systems (Figures 6a and 6b); however, it is unlikely that these dictate strain behavior across the larger fault array. Instead, our results suggest that during the early stages of rifting changes in extension rate have significant control on strain behavior. We argue that relatively low and decreasing extension rates (14 m/Myr) lead to an interrift period that is characterized by distributed faulting and local synrift cooling (Pre-Triassic to Late Triassic) (Figures 12a–12d). Relatively high and increasing extension rates (from 16 m/Myr, Early Jurassic, to 89 m/Myr, Middle to Late Jurassic, Figure 5d) lead to a heterogeneous strain distribution and, in the case of the East Shetland Basin, the gradual transition from lithospheric stretching to thinning, and ultimately to rift narrowing (Figures 12e–12h). Our results are qualitatively consistent with the previous results from natural rifts and predictions of rift models that investigate the effect extension rate on the rift pattern development.

This study illustrates the importance of the detailed analyses using regionally extensive, high-resolution 3-D subsurface data over a considerable period of basin development, which results provide observations that can be compared with numerical rift analogs. Studies that propose a simple or multiphase rift evolution with a homogeneous strain distribution or directional strain migration pattern based on less extensive analyses across the full extent of the basin possibly overlook fault array development and local strain accumulations, especially during periods of relatively less rift activity. Heterogeneous three-dimensional strain behavior during the initial phases of continental rifting as a result of varying extension rate and magnitude are not typically generated in simple rift models yet can be a significant aspect of rift dynamics.

Data Availability Statement

The data used for this study are publically available for download via the U.K. National Data Repository (NDR) (<https://ndr.ogauthority.co.uk>) for the U.K. side and the DISKOS online portal (Diskos) (<https://portal.diskos.cgg.com>) for the Norwegian side (see supporting information).

References

- Badley, M. E., Price, J. D., Dahl, C. R., & Agdestein, T. (1988). The structural evolution of the northern Viking Graben and its bearing upon extensional modes of basin formation. *Journal of the Geological Society*, *145*(3), 455–472. <https://doi.org/10.1144/gsjgs.145.3.0455>
- Bassi, G. (1991). Factors controlling the style of continental rifting: Insights from numerical modelling. *Earth and Planetary Science Letters*, *105*(4), 430–452. [https://doi.org/10.1016/0012-821X\(91\)90183-I](https://doi.org/10.1016/0012-821X(91)90183-I)
- Bassi, G. (1995). Relative importance of strain rate and rheology for the mode of continental extension. *Geophysical Journal International*, *122*(1), 195–210. <https://doi.org/10.1111/j.1365-246X.1995.tb03547.x>
- Bayona, G., & Thomas, W. A. (2003). Distinguishing fault reactivation from flexural deformation in the distal stratigraphy of the peripheral Blountian foreland basin, southern Appalachians, USA. *Basin Research*, *15*(4), 503–526. <https://doi.org/10.1046/j.1365-2117.2003.00217.x>

Acknowledgments

We acknowledge funding from the Equinor Departmental Scholarship at Imperial College London and the MultiRift Project, which is funded by the Research Council of Norway (PETROMAKS Project 215591) and Equinor (data provider/supporter) to the University of Bergen, and partners Imperial College London, University of Manchester, and University of Oslo. We thank Editor Laurent Jolivet, Douglas Paton, Emmanuel Masini, and an anonymous reviewer for their constructive reviews. Al Fraser and Jon Bull are thanked for their comments on the initial version of this work. For their involvement in providing the data and permission to publish, we are grateful Thomas Weight, Tom Dreyer, Mark Lawson, Claire Thomas, and Bart Hendriks at Equinor, Richard Lamb and Emma Taylor at PGS, and Bent Kjøllhamar at TGS. Schlumberger is thanked for providing Petrel to Imperial College London and the Earthquake Research Institute of The University of Tokyo. We also thank the members of the Basins Research Group at Imperial College London and the MultiRift Project, in particular Thilo Wrona, for fruitful discussions.

- Behn, M. D., Lin, J., & Zuber, M. T. (2002). A continuum mechanics model for normal faulting using a strain-rate softening rheology: Implications for thermal and rheological controls on continental and oceanic rifting. *Earth and Planetary Science Letters*, *202*(3–4), 725–740. [https://doi.org/10.1016/S0012-821X\(02\)00792-6](https://doi.org/10.1016/S0012-821X(02)00792-6)
- Bell, R. E., Jackson, C. A.-L., Whipp, P. S., & Clements, B. (2014). Strain migration during multiphase extension: Observations from the northern North Sea. *Tectonics*, *33*, 1936–1963. <https://doi.org/10.1002/2014TC003551>
- Bell, R. E., McNeill, L. C., Bull, J. M., Henstock, T. J., Collier, R. L., & Leeder, M. R. (2009). Fault architecture, basin structure and evolution of the Gulf of Corinth Rift, central Greece. *Basin Research*, *21*(6), 824–855. <https://doi.org/10.1111/j.1365-2117.2009.00401.x>
- Bellingham, P., & White, N. (2000). A general inverse method for modelling extensional sedimentary basins. *Basin Research*, *12*(3–4), 219–226. <https://doi.org/10.1111/j.1365-2117.2000.00122.x>
- Bendick, R., McClusky, S., Bilham, R., Asfaw, L., & Klemperer, S. (2006). Distributed Nubia-Somalia relative motion and dike intrusion in the Main Ethiopian Rift. *Geophysical Journal International*, *165*(1), 303–310. <https://doi.org/10.1111/j.1365-246X.2006.02904.x>
- Bouroulllec, R., Cartwright, J. A., Johnson, H. D., Lansigu, C., Quémener, J. M., & Savanier, D. (2004). *Syn depositional faulting in the Grès d'Annot Formation, SE France: High-resolution kinematic analysis and stratigraphic response to growth faulting*, Special Publications (Vol. 221, pp. 241–265). London: Geological Society. <https://doi.org/10.1144/GSL.SP.2004.221.01.13>
- Brun, J.-P. (1999). Narrow rifts versus wide rifts: Inferences for the mechanics of rifting from laboratory experiments. *Philosophical Transactions of the Royal Society of London, Series A: Mathematical, Physical and Engineering Sciences*, *357*(1753), 695–712. <https://doi.org/10.1098/rsta.1999.0349>
- Brune, S., Williams, S. E., Butterworth, N. P., & Müller, R. D. (2016). Abrupt plate accelerations shape rifted continental margins. *Nature*, *536*(7615), 201–204. <https://doi.org/10.1038/nature18319>
- Buck, W. R. (1991). Modes of continental lithospheric extension. *Journal of Geophysical Research*, *96*(B12), 20,161–20,178. <https://doi.org/10.1029/91JB01485>
- Buck, W. R. (2006). *The role of magma in the development of the Afro-Arabian Rift System*, Special Publications (Vol. 259, pp. 43–54). London: Geological Society. <https://doi.org/10.1144/GSL.SP.2006.259.01.05>
- Calais, E., Lesne, O., Déverchère, J., San'kov, V., Lukhnev, A., Miroshnichenko, A., et al. (1998). Crustal deformation in the Baikal rift from GPS measurements. *Geophysical Research Letters*, *25*(21), 4003–4006. <https://doi.org/10.1029/1998GL900067>
- Cartwright, J., Bouroulllec, R., James, D., & Johnson, H. (1998). Polycyclic motion history of some Gulf Coast growth faults from high-resolution displacement analysis. *Geology*, *26*(9), 819–822. [https://doi.org/10.1130/0091-7613\(1998\)026<0819:PMHOSG>2.3.CO;2](https://doi.org/10.1130/0091-7613(1998)026<0819:PMHOSG>2.3.CO;2)
- Claringbould, J. S., Bell, R. E., Jackson, C. A.-L., Gawthorpe, R. L., & Odinsen, T. (2017). Pre-existing normal faults have limited control on the rift geometry of the northern North Sea. *Earth and Planetary Science Letters*, *475*, 190–206. <https://doi.org/10.1016/j.epsl.2017.07.014>
- Corti, G., Bonini, M., Conticelli, S., Innocenti, F., Manetti, P., & Sokoutis, D. (2003). Analogue modelling of continental extension: A review focused on the relations between the patterns of deformation and the presence of magma. *Earth-Science Reviews*, *63*(3–4), 169–247. [https://doi.org/10.1016/S0012-8252\(03\)00035-7](https://doi.org/10.1016/S0012-8252(03)00035-7)
- Corti, G., Ranalli, G., Agostini, A., & Sokoutis, D. (2013). Inward migration of faulting during continental rifting: Effects of pre-existing lithospheric structure and extension rate. *Tectonophysics*, *594*, 137–148. <https://doi.org/10.1016/j.tecto.2013.03.028>
- Cowie, P. A., Gupta, S., & Dawers, N. H. (2000). Implications of fault array evolution for synrift depocentre development: Insights from a numerical fault growth model. *Basin Research*, *37*(7), 2221–2242. <https://doi.org/10.1029/2017TC004776>
- Cowie, P. A., Underhill, J. R., Behn, M. D., Lin, J., & Gill, C. E. (2005). Spatio-temporal evolution of strain accumulation derived from multi-scale observations of Late Jurassic rifting in the northern North Sea: A critical test of models for lithospheric extension. *Earth and Planetary Science Letters*, *234*(3–4), 401–419. <http://doi.org/10.1016/j.epsl.2005.01.039>
- Duffy, O. B., Bell, R. E., Jackson, C. A.-L., Gawthorpe, R. L., & Whipp, P. S. (2015). Fault growth and interactions in a multiphase rift fault network: Horda Platform, Norwegian North Sea. *Journal of Structural Geology*, *80*, 99–119. <https://doi.org/10.1016/j.jsg.2015.08.015>
- England, P. (1983). Constraints on extension of continental lithosphere. *Journal of Geophysical Research*, *88*(B2), 1145–1152. <https://doi.org/10.1029/JB088iB02p01145>
- Færseth, R. B. (1996). Interaction of Permo-Triassic and Jurassic extensional fault-blocks during the development of the northern North Sea. *Journal of the Geological Society*, *153*(6), 931–944. <https://doi.org/10.1144/gsjgs.153.6.0931>
- Færseth, R. B., Sjøblom, T. S., Steel, R. J., Liljedahl, T., Saunar, B. E., & Tjelland, T. (1995). *Tectonic controls on Bathonian-Volgian syn-rift successions on the Visund fault block, northern North Sea*. In *Norwegian Petroleum Society Special Publications* (Vol. 5, pp. 325–346). Cambridge, UK: Elsevier. [https://doi.org/10.1016/S0928-8937\(06\)80074-3](https://doi.org/10.1016/S0928-8937(06)80074-3)
- Ford, M., Rohais, S., Williams, E. A., Bourlange, S., Jousset, D., Backert, N., & Malartre, F. (2013). Tectono-sedimentary evolution of the western Corinth rift (Central Greece). *Basin Research*, *25*(1), 3–25. <https://doi.org/10.1111/j.1365-2117.2012.00550.x>
- Fossen, H. (2010). *Structural geology*. Cambridge, UK: Cambridge University Press. <https://doi.org/10.1017/CBO9780511777806>
- Gawthorpe, R. L., & Leeder, M. R. (2000). Tectono-sedimentary evolution of active extensional basins. *Basin Research*, *12*(3–4), 195–218. <https://doi.org/10.1111/j.1365-2117.2000.00121.x>
- Giba, M., Walsh, J. J., & Nicol, A. (2012). Segmentation and growth of an obliquely reactivated normal fault. *Journal of Structural Geology*, *39*, 253–267. <https://doi.org/10.1016/j.jsg.2012.01.004>
- Gibbs, A. D. (1984). Structural evolution of extensional basin margins. *Journal of the Geological Society*, *141*(4), 609–620. <https://doi.org/10.1144/gsjgs.141.4.0609>
- Henstra, G. A., Berg Kristensen, T., Rotevatn, A., & Gawthorpe, R. L. (2019). How do pre-existing normal faults influence rift geometry? A comparison of adjacent basins with contrasting underlying structure on the Lofoten Margin, Norway. *Basin Research*, *31*(6), 1083–1097. <https://doi.org/10.1111/bre.12358>
- Houseman, G., & England, P. (1986). A dynamical model of lithosphere extension and sedimentary basin formation. *Journal of Geophysical Research*, *91*(B1), 719–729. <https://doi.org/10.1029/JB091iB01p00719>
- Huisman, R. S., & Beaumont, C. (2007). *Roles of lithospheric strain softening and heterogeneity in determining the geometry of rifts and continental margins*, Special Publications (Vol. 282, pp. 111–138). London: Geological Society. <https://doi.org/10.1144/SP282.6>
- Huisman, R. S., Podladchikov, Y. Y., & Cloetingh, S. A. P. L. (2001). Transition from passive to active rifting: Relative importance of asthenospheric doming and passive extension of the lithosphere. *Journal of Geophysical Research*, *106*(B6), 11,271–11,291. <https://doi.org/10.1029/2000JB900424>
- Jackson, C. A.-L., Bell, R. E., Rotevatn, A., & Tvedt, A. B. (2017). *Techniques to determine the kinematics of synsedimentary normal faults and implications for fault growth models*, Special Publications (Vol. 439, pp. 187–217). London: Geological Society. <https://doi.org/10.1144/SP439.22>
- Jackson, C. A.-L., & Rotevatn, A. (2013). 3D seismic analysis of the structure and evolution of a salt-influenced normal fault zone: A test of competing fault growth models. *Journal of Structural Geology*, *54*, 215–234. <https://doi.org/10.1016/j.jsg.2013.06.012>

- Kusznr, N. J., & Park, R. G. (1987). *The extensional strength of the continental lithosphere: Its dependence on geothermal gradient, and crustal composition and thickness*, *Special Publications* (Vol. 28, pp. 35–52). London: Geological Society. <https://doi.org/10.1144/GSL.SP.1987.028.01.04>
- Lee, M. J., & Hwang, Y. J. (1993). *Tectonic evolution and structural styles of the East Shetland Basin*, *Petroleum Geology Conference Series* (Vol. 4, pp. 1137–1149). London: Geological Society. <https://doi.org/10.1144/0041137>
- Lewis, M. M., Jackson, C. A.-L., & Gawthorpe, R. L. (2013). Salt-influenced normal fault growth and forced folding: The Stavanger Fault System, North Sea. *Journal of Structural Geology*, *54*, 156–173. <https://doi.org/10.1016/j.jsg.2013.07.015>
- McClay, K. R. (1990). Extensional fault systems in sedimentary basins: A review of analogue model studies. *Marine and Petroleum Geology*, *7*(3), 206–233. [https://doi.org/10.1016/0264-8172\(90\)90001-W](https://doi.org/10.1016/0264-8172(90)90001-W)
- McClusky, S., Reilinger, R., Ogubazghi, G., Amleson, A., Healeb, B., Vernant, P., et al. (2010). Kinematics of the southern Red Sea-Afar Triple Junction and implications for plate dynamics. *Geophysical Research Letters*, *37*, L05301. <https://doi.org/10.1029/2009GL041127>
- McLeod, A. E., Dawers, N. H., & Underhill, J. R. (2000). The propagation and linkage of normal faults: Insights from the Strathspey-Brent-Stafford fault array, northern North Sea. *Basin Research*, *12*(3–4), 263–284. <https://doi.org/10.1111/j.1365-2117.2000.00124.x>
- McLeod, A. E., Underhill, J. R., Davies, S. J., & Dawers, N. H. (2002). The influence of fault array evolution on synrift sedimentation patterns: Controls on deposition in the Strathspey-Brent-Stafford half graben, northern North Sea. *AAPG Bulletin*, *86*(6), 1061–1093. <https://doi.org/10.1306/61EEDC24-173E-11D7-8645000102C1865D>
- Nagel, T. J., & Buck, W. R. (2007). Control of rheological stratification on rifting geometry: A symmetric model resolving the upper plate paradox. *International Journal of Earth Sciences*, *96*(6), 1047–1057. <https://doi.org/10.1007/s00531-007-0195-x>
- Naliboff, J. B., & Buitter, S. J. H. (2015). Rift reactivation and migration during multiphase extension. *Earth and Planetary Science Letters*, *421*, 58–67. <https://doi.org/10.1016/j.epsl.2015.03.050>
- Naliboff, J. B., Buitter, S. J. H., Péron-Pinvidic, G., Osmundsen, P. T., & Tetreault, J. L. (2017). Complex fault interaction controls continental rifting. *Nature Communications*, *8*(1), 1179. <https://doi.org/10.1038/s41467-017-00904-x>
- Newman, R., & White, N. (1999). The dynamics of extensional sedimentary basins: Constraints from subsidence inversion. *Philosophical transactions of the Royal Society of London. Series A: Mathematical, Physical and Engineering Sciences*, *357*(1753), 805–834. <https://doi.org/10.1098/rsta.1999.0353>
- Nixon, C. W., Bull, J. M., & Sanderson, D. J. (2014). Localized vs distributed deformation associated with the linkage history of an active normal fault, Whakatane Graben, New Zealand. *Journal of Structural Geology*, *69*, 266–280. <https://doi.org/10.1016/j.jsg.2014.06.005>
- Nixon, C. W., McNeill, L. C., Bull, J. M., Bell, R. E., Gawthorpe, R. L., Henstock, T. J., et al. (2016). Rapid spatiotemporal variations in rift structure during development of the Corinth Rift, central Greece. *Tectonics*, *35*, 1225–1248. <https://doi.org/10.1002/2015TC004026>
- Odinsen, T., Reemst, P., Van der Beek, P., Faleide, J. I., & Gabrielsen, R. H. (2000). *Permo-Triassic and Jurassic extension in the northern North Sea: Results from tectonostratigraphic forward modelling*, *Special Publications* (Vol. 167, pp. 83–103). London: Geological Society. <https://doi.org/10.1144/GSL.SP.2000.167.01.05>
- Paton, D. A. (2006). Influence of crustal heterogeneity on normal fault dimensions and evolution: Southern South Africa extensional system. *Journal of Structural Geology*, *28*(5), 868–886. <https://doi.org/10.1016/j.jsg.2006.01.006>
- Patrino, S., & Reid, W. (2017). New plays on the Greater East Shetland Platform (UKCS Quadrants 3, 8–9, 14–16)—part 2: Newly reported Permo-Triassic intra-platform basins and their influence on the Devonian-Paleogene prospectivity of the area. *First Break*, *35*(1), 59–69.
- Péron-Pinvidic, G., Manatschal, G., & Osmundsen, P. T. (2013). Structural comparison of archetypal Atlantic rifted margins: A review of observations and concepts. *Marine and Petroleum Geology*, *43*, 21–47. <https://doi.org/10.1016/j.marpetgeo.2013.02.002>
- Phillips, T. B., Fazlikhani, H., Gawthorpe, R. L., Fossen, H., Jackson, C. A. L., Bell, R. E., et al. (2019). The influence of structural inheritance and multiphase extension on rift development, the Northern North Sea. *Tectonics*, *38*, 4099–4126. <https://doi.org/10.1029/2019TC005756>
- Phillips, T. B., Jackson, C. A.-L., Bell, R. E., Duffy, O. B., & Fossen, H. (2016). Reactivation of intrabasement structures during rifting: A case study from offshore southern Norway. *Journal of Structural Geology*, *91*, 54–73. <https://doi.org/10.1016/j.jsg.2016.08.008>
- Putz-Perrier, M. W., & Sanderson, D. J. (2008). *The distribution of faults and fractures and their importance in accommodating extensional strain at Kimmeridge Bay, Dorset, UK*, *Special Publications* (Vol. 299, pp. 97–111). London: Geological Society. <https://doi.org/10.1144/SP299.6>
- Ravnås, R., Nøttvedt, A., Steel, R. J., & Windelstad, J. (2000). *Syn-rift sedimentary architectures in the northern North Sea*, *Special Publications* (Vol. 167, pp. 133–177). London: Geological Society. <https://doi.org/10.1144/GSL.SP.2000.167.01.07>
- Reeve, M. T., Bell, R. E., Duffy, O. B., Jackson, C. A. L., & Sansom, E. (2015). The growth of non-colinear normal fault systems; what can we learn from 3D seismic reflection data? *Journal of Structural Geology*, *70*, 141–155. <https://doi.org/10.1016/j.jsg.2014.11.007>
- Roberts, A. M., Yielding, G., Kusznr, N. J., Walker, I. M., & Dorn-Lopez, D. (1993). *Mesozoic extension in the North Sea: Constraints from flexural backstripping, forward modelling and fault populations*, *Petroleum Geology Conference Series* (Vol. 4, pp. 1123–1136). London: Geological Society. <https://doi.org/10.1144/0041123>
- Roberts, A. M., Yielding, G., Kusznr, N. J., Walker, I. M., & Dorn-Lopez, D. (1995). Quantitative analysis of Triassic extension in the northern Viking Graben. *Journal of the Geological Society*, *152*(1), 15–26. <https://doi.org/10.1144/gsjgs.152.1.0015>
- Soliva, R., Benedicto, A., & Maerten, L. (2006). Spacing and linkage of confined normal faults: Importance of mechanical thickness. *Journal of Geophysical Research*, *111*, B01402. <https://doi.org/10.1029/2004JB003507>
- Stab, M., Bellahsen, N., Pik, R., Quidelleur, X., Ayalew, D., & Leroy, S. (2016). Modes of rifting in magma-rich settings: Tectono-magmatic evolution of Central Afar. *Tectonics*, *35*, 2–38. <https://doi.org/10.1002/2015TC003893>
- Taylor, S. K., Nicol, A., & Walsh, J. J. (2008). Displacement loss on growth faults due to sediment compaction. *Journal of Structural Geology*, *30*(3), 394–405. <https://doi.org/10.1016/j.jsg.2007.11.006>
- Tetreault, J. L., & Buitter, S. J. H. (2018). The influence of extension rate and crustal rheology on the evolution of passive margins from rifting to break-up. *Tectonophysics*, *746*, 155–172. <https://doi.org/10.1016/j.tecto.2017.08.029>
- Thomas, D. W., & Coward, M. P. (1995). Late Jurassic-Early Cretaceous inversion of the northern east Shetland Basin, northern North Sea. *Geological Society, London, Special Publications*, *88*(1), 275–306. <https://doi.org/10.1144/GSL.SP.1995.088.01.16>
- Thorsen, C. E. (1963). Age of growth faulting in the southeast Louisiana. *Transactions. Gulf Coast Association of Geological Societies*, *13*, 103–110.
- Tomasso, M., Underhill, J. R., Hodgkinson, R. A., & Young, M. J. (2008). Structural styles and depositional architecture in the Triassic of the Ninian and Alwyn North fields: Implications for basin development and prospectivity in the northern North Sea. *Marine and Petroleum Geology*, *25*(7), 588–605. <https://doi.org/10.1016/j.marpetgeo.2007.11.007>

- Tvedt, A. B., Rotevatn, A., Jackson, C. A. L., Fossen, H., & Gawthorpe, R. L. (2013). Growth of normal faults in multilayer sequences: A 3D seismic case study from the Egersund Basin, Norwegian North Sea. *Journal of Structural Geology*, *55*, 1–20. <https://doi.org/10.1016/j.jsg.2013.08.002>
- Van Wijk, J. W., & Cloetingh, S. A. P. L. (2002). Basin migration caused by slow lithospheric extension. *Earth and Planetary Science Letters*, *198*(3–4), 275–288. [https://doi.org/10.1016/S0012-821X\(02\)00560-5](https://doi.org/10.1016/S0012-821X(02)00560-5)
- Walsh, J. J., Bailey, W. R., Childs, C., Nicol, A., & Bonson, C. G. (2003). Formation of segmented normal faults: A 3-D perspective. *Journal of Structural Geology*, *25*(8), 1251–1262. [https://doi.org/10.1016/S0191-8141\(02\)00161-X](https://doi.org/10.1016/S0191-8141(02)00161-X)
- Walsh, J. J., & Watterson, J. (1992). Populations of faults and fault displacements and their effects on estimates of fault-related regional extension. *Journal of Structural Geology*, *14*(6), 701–712. [https://doi.org/10.1016/0191-8141\(92\)90127-1](https://doi.org/10.1016/0191-8141(92)90127-1)
- Whipp, P. S., Jackson, C. A.-L., Gawthorpe, R. L., Dreyer, T., & Quinn, D. (2014). Normal fault array evolution above a reactivated rift fabric; a subsurface example from the northern Horda Platform, Norwegian North Sea. *Basin Research*, *26*(4), 523–549. <https://doi.org/10.1111/bre.12050>
- Wolfenden, E., Ebinger, C., Yirgu, G., Renne, P. R., & Kelley, S. P. (2005). Evolution of a volcanic rifted margin: Southern Red Sea, Ethiopia. *Geological Society of America Bulletin*, *117*(7), 846–864. <https://doi.org/10.1130/B25516.1>
- Young, M. J., Gawthorpe, R. L., & Hardy, S. (2001). Growth and linkage of a segmented normal fault zone; the Late Jurassic Murchison-Statfjord North Fault, northern North Sea. *Journal of Structural Geology*, *23*(12), 1933–1952. [https://doi.org/10.1016/S0191-8141\(01\)00038-4](https://doi.org/10.1016/S0191-8141(01)00038-4)
- Ziegler, P. A., & Cloetingh, S. (2004). Dynamic processes controlling evolution of rifted basins. *Earth-Science Reviews*, *64*(1–2), 1–50. [https://doi.org/10.1016/S0012-8252\(03\)00041-2](https://doi.org/10.1016/S0012-8252(03)00041-2)

References From the Supporting Information

- Childs, C., Easton, S. J., Vendeville, B. C., Jackson, M. P. A., Lin, S. T., Walsh, J. J., & Watterson, J. (1993). Kinematic analysis of faults in a physical model of growth faulting above a viscous salt analogue. *Tectonophysics*, *228*(3–4), 313–329. [https://doi.org/10.1016/0040-1951\(93\)90346-L](https://doi.org/10.1016/0040-1951(93)90346-L)
- Claringbould, J. S. (2015). Structural and stratigraphic expression of multiphase extension in rift basins, (Doctoral dissertation). Retrieved from Spiral (<http://hdl.handle.net/10044/1/51557>). London, UK: Imperial College London.
- Hongxing, G., & Anderson, J. K. (2007). Fault throw profile and kinematics of normal fault: Conceptual models and geologic examples. *Geological Journal of China Universities*, *13*, 75–88.
- Taylor, S. K., Bull, J. M., Lamarche, G., & Barnes, P. M. (2004). Normal fault growth and linkage in the Whakatane Graben, New Zealand, during the last 1.3 Myr. *Journal of Geophysical Research*, *109*, B02408. <https://doi.org/10.1029/2003JB002412>
- ten Veen, J. H., & Kleinspehn, K. L. (2000). Quantifying the timing and sense of fault dip slip: New application of biostratigraphy and geohistory analysis. *Geology*, *28*(5), 471–474. [https://doi.org/10.1130/0091-7613\(2000\)28<471:QTTASO>2.0.CO;2](https://doi.org/10.1130/0091-7613(2000)28<471:QTTASO>2.0.CO;2)
- Walsh, J. J., Nicol, A., & Childs, C. (2002). An alternative model for the growth of faults. *Journal of Structural Geology*, *24*(11), 1669–1675. [https://doi.org/10.1016/S0191-8141\(01\)00165-1](https://doi.org/10.1016/S0191-8141(01)00165-1)